IMPROVED DROUGHT EARLY WARNING AND FORECASTING TO STRENGTHEN PREPAREDNESS AND ADAPTATION TO DROUGHTS IN AFRICA

DEWFORA

A 7th Framework Programme Collaborative Research Project

Skill of the multi-model forecasting system in predicting variables and drought indicators

WP4-D4.2

December 2011

Coordinator:	Deltares, The Netherlands
Project website:	www.dewfora.net
FP7 Call	ENV-2010-1.3.3.1
Contract no.	265454

Page intentionally left blank

DOCUMENT INFORMATION

Title	Skill of the multi-model forecasting system in predicting variables and drought indicators
Lead Author	ECMWF
Contributors	CSIR
Distribution	PU: Public
Reference	WP4-D4.2

DOCUMENT HISTORY

Date	Revision	Prepared by	Organisation	Approved by	Notes
09/12/2011	V0				Draft version v0
14/12/2011	V1				Draft version v1
21/12/2011	Final	Emanuel Dutra Florian Pappenberger Fredrik Wetterhall Willem Landman	ECMWF CSIR	Micha Werner	Final version

ACKNOWLEDGEMENT

The research leading to these results has received funding from the European Union's Seventh Framework Programme (FP7/2007-2013) under grant agreement N°265454.

Page intentionally left blank

SUMMARY

This report presents an evaluation of the skill of different seasonal forecasts systems and a multi-model composite to predict precipitation. The report has three chapters addressing: i) quality and availability of precipitation datasets to be used for drought monitoring in Africa; ii) skill of seasonal forecasts of precipitation in Africa, and iii) a case study of the integration of monitoring and forecasting for the recent 2010-11 drought in the Horn of Africa.

The comparison of four global precipitation datasets over Africa and ECMWF ERA-Interim (ERAI) reanalysis highlight the uncertainty of those datasets for verification purposes. It was found that the use of ERAI precipitation has limitations for drought applications, especially over the tropical rainforest, because of drifts in the model climate. However, in the other regions, it compares reasonable well with the remaining datasets and has the potential to be used as a monitoring tool because of its near real time update (in contrast with the other datasets). Furthermore, a robust evaluation of seasonal forecasts is dependent on the verification dataset. Since there is no clear information on which dataset is more reliable, the seasonal forecasts of precipitation were verified against GPCPv2.2.

Forecast skill is usually highest when considering multi-model ensemble (MME) forecasts, created by combining forecasts from several different models. Here we evaluate four seasonal forecast systems: ECMWF system 3 (S3) and system 4 (S4), the Met Office (UK) and Météo-France (MF). Our results suggest that the MME does not consistently outperform any particular model. Although this could seem inconsistent with some literature, in this case the MME is a composite of only 4 systems, while most of the MME works combine more systems. Furthermore, S3 will be discontinued during 2012 and the UK system used in this report is an older version of the current system in operations. For these reasons, S4 is the only viable seasonal forecast system, produced by ECMWF, which can be used in DEWFORA.

The 2010-11 drought in the Horn of Africa resulted from a precipitation deficit in both the Oct-Dec 2010 and Mar-May 2011 rainy seasons, and this was captured by ERAI. Soil moisture anomalies of ERAI also indentified the onset of the drought condition early in Oct 2010 with a persistent drought still present in Sep 2011. The precipitation deficit in Oct-Dec 2010 was associated with a strong La Niña event. The ECMWF seasonal forecasts of NINO3.4 predicted the La Niña event from June 2010 onwards, and also a dry precipitation anomaly for the region from July 2010 onwards. On the other hand, the seasonal forecasts for the Mar-May 2011 season did not predict the anomaly in advance, except for the forecasts in March 2011.

This report is an extension of D4.1 and future reports will include the skill of seasonal forecasts of drought indexes as well as statistical methods to estimate drought indicators.

Page intentionally left blank

TABLE OF CONTENTS

LIST OF FIGURES

LIST OF TABLES

Page intentionally left blank

1. INTRODUCTION

Seasonal prediction using coupled dynamical models has progressed significantly over the last 20 years. Starting from coupled atmosphere-ocean models of intermediate complexity and spanning the tropical domain (Cane et al. 1986), seasonal prediction has become an operational activity using comprehensive coupled ocean-atmosphere models spanning the global domain. However, its application to drought forecasts is still in the early stages.

Drought is a major natural hazard with serious impacts on society. The determination of drought magnitude in real time (monitoring) is dependent on available and reliable observations/model estimates, and can be as complicated as the definition of drought. Not only is drought differentiated from other natural disasters by its many and diverse impacts, but it is also related with its spatial extend, intensity, magnitude, and duration (Svoboda et al. 2002).

This report follows the D4.1 DEWFORA report, evaluating the skill of different seasonal forecasts systems and a multi-model composite in predicting variables related to drought indicators, namely precipitation. In this report we only address the direct use of global circulation models output, whereas dynamical and statistical downscaling methods to estimate drought indicators will be included in future reports. The report has three chapters addressing: i) quality and availability of precipitation datasets to be used for drought monitoring in Africa; ii) skill of seasonal forecasts of precipitation in Africa, and iii) a case study of the integration of monitoring and forecasting for the recent 2010-11 drought in the Horn of Africa. Although the Horn of Africa is not a case study of DEWFORA, we present it due to the impact of the recent drought on the population and as an example of the potential of monitoring and forecasting droughts using global circulation models.

2. GLOBAL PRECIPITATION PRODUCTS IN AFRICA

Rainfall plays a major role in determining agricultural production in areas dependent on traditional rainfed agriculture, and a persistent anomaly in this precipitation is thought to be the main cause of drought in those regions. However, in-situ observations of precipitation over continental Africa are scarce. This is a limitation when validating numerical weather prediction. In this chapter we compare several global datasets of precipitation over Africa to identify uncertainties, and select a dataset to verify the seasonal forecasts.

2.1 REGIONS AND DATASETS

The observation-based precipitation datasets in this study include: i) the Global Precipitation Climatology Centre version 4 (GPCCv4, Fuchs and al. 2009); ii) the Climate Prediction Center (CPC) Merged Analysis of Precipitation (CMAP, Xie and Arkin 1997); iii) the Global Precipitation Climatology Project versions 2.1 and 2.2 (GPCPv2.1/2 Huffman et al. 2009) and; GPCC is only based in rain-gauges, while GPCP and CMAP blend data from a variety of satellites and gauges.

From numerical weather prediction models, we selected the ECMWF ERA-Interim reanalysis, the latest global atmospheric reanalysis produced by ECMWF which extends from 1 January 1979 to the present date. See *Dee et al. (2011)* for detailed descriptions of the atmospheric model used in ERAI, the data assimilation system, the observations used, and various performance aspects. The ERAI configuration has a spectral T255 horizontal resolution (about 0.7°x0.7° in the grid-point space) with 60 model levels. For comparison purposes the previous ECWMF ERA40 reanalysis (Uppala et al. 2005) (1.125°x1.125°) was also included. Both ERAI and ERA40 precipitation were taken from the first 12hr forecasts starting at 00UTC and 12UTC daily. This is the forecast window closest to the initial conditions provided by the data assimilation system; however these should be considered as short-range forecasts and not analysis.

In the following analysis (and also seasonal forecasts) the evaluation of precipitation is performed over different regions (Figure 1 and Table 1). The regions definitions were adapted from Di Giuseppe et al. (2011). They applied a *k-mean* clustering algorithm to GPCPv2.1 in order to identify regions with homogeneous precipitation climatologies. Further details of the method are given by Di Giuseppe et al. (2011). The GCPC and CMAP datasets are available in a 2.5°x2.5° latitude/longitude grid while the other datasets have higher resolutions. To standardize the regions definitions it was decided to interpolate (mass conservative) all the datasets to the coarser 2.5°x2.5° grid.

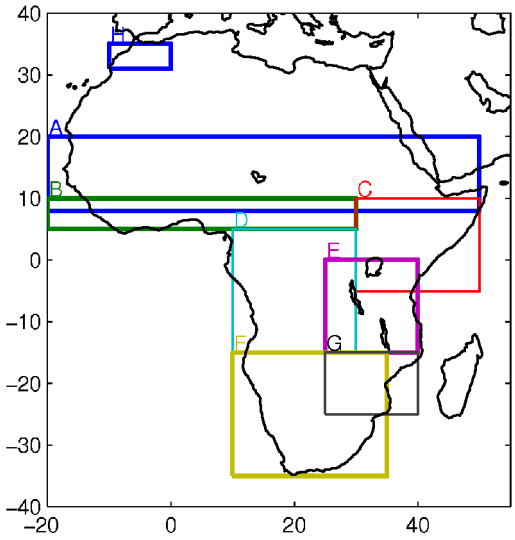

Figure 1. Africa regions adapted from Giuseppe et al. (2011).

Table 1. Africa regions definition of longitude and latitude, land only area and number of land grid points on the 2.5°x2.5° grid. Region H differs from Di Giuseppe et al. (2011) definition (they included Madagascar), to include a region surrounding the Oum-er-Rbia River Basin.

Region	Longitude; Latitude	Area (x10^6 km^2)	N. points
A	[-20,50] E; [8,20]N	8.9	119
B	[-20,30]E; [5,10]N	2.4	31
C	[30,50]E; [-5,10]N	2.5	32
D	[10,30]E; [-15,5]N	4.4	57
E	[25,40]E; [-15,0]N	2.4	32
F	[10,35]E; [-35,-15]N	3.6	51
G	[25,40]E; [-25,-15]N	1.3	18
H	[-10,0]E; [31,35]N	0.4	6
AF	[-20,50]E; [-35,35]N	29.7	407

The mean spatial patterns of annual precipitation from the different datasets (Figure 2) agree on the dry/wet north/south gradient from the desert areas to the tropical savannas and rainforests. However, it is possible to identify a tendency of the reanalysis products (both ERAI and ERA40) to overestimate precipitation in the tropical rainforests.

The mean annual cycle of precipitation evaluated for the different regions (Table 1) is represented in Figure 3. It is possible to identify some regions where there is a large uncertainty among the different datasets: B, C, H, and Africa as a whole (AF). The tendency of the reanalyses to overestimate the peak rainfall is evident in areas B and D.

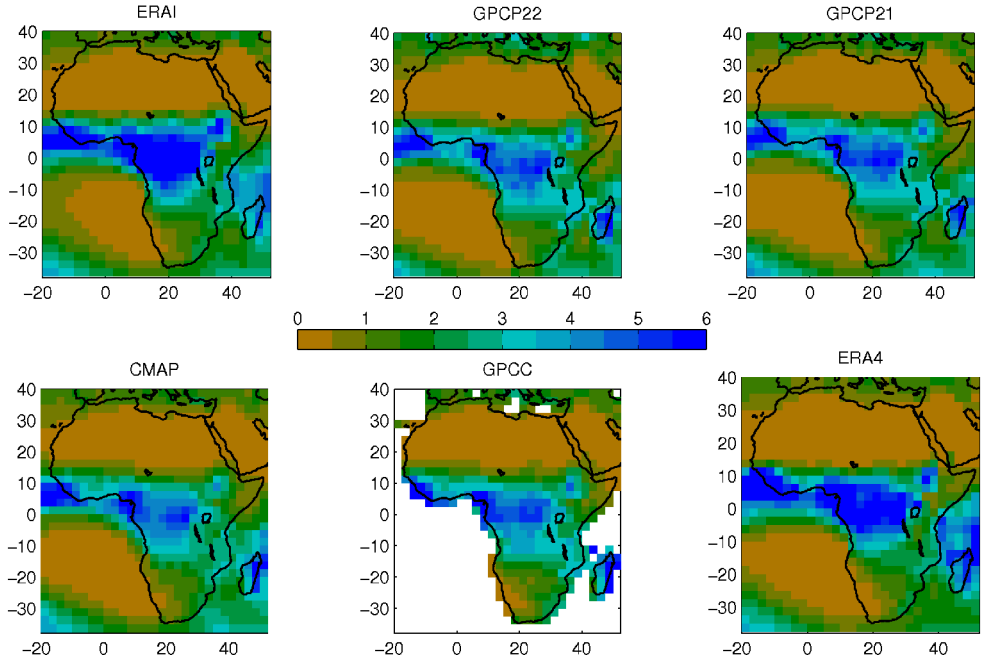

Figure 2. Mean annual precipitation (mm day^{-1}) from ERA-Interim, GPCPv2.2, GPCPv2.1, CMAP, GPCC and ERA-40. The mean refers to the common period 1979 to 2008 (to 2001 in the case of ERA-40).

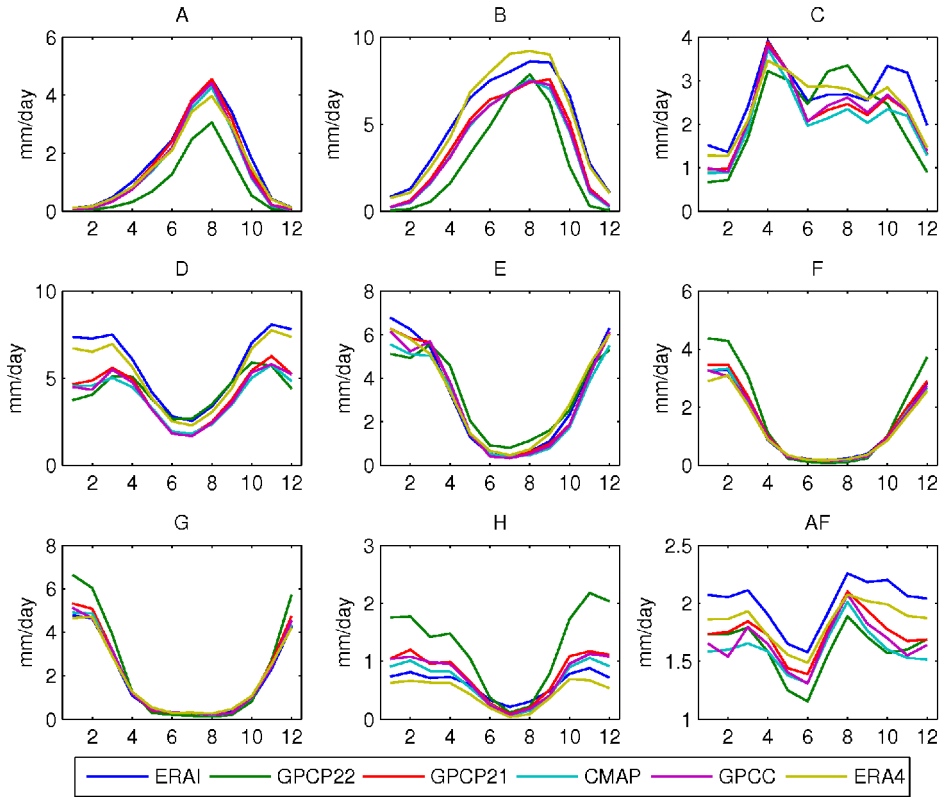

Figure 3. Mean annual cycle of precipitation from the different products averaged over the nine regions in Africa defined in Table 1 and Figure 1.

2.2 DROUGHT INDICES

The standardized precipitation index (SPI) (Mckee et al. 1993) is one of the simplest drought indicators. SPI is computed by fitting a probability density function to a frequency distribution of precipitation summed over the time scale of interest: SPI3 (3 months), SP6 (6 months),

SPI12 (12 months). This is performed separately for each month and for each location. The SPI is a commonly used drought index (Keyantash and Dracup 2002) and recommended by the World Meteorological Organization as a standard to characterize meteorological droughts (WMO 2009).

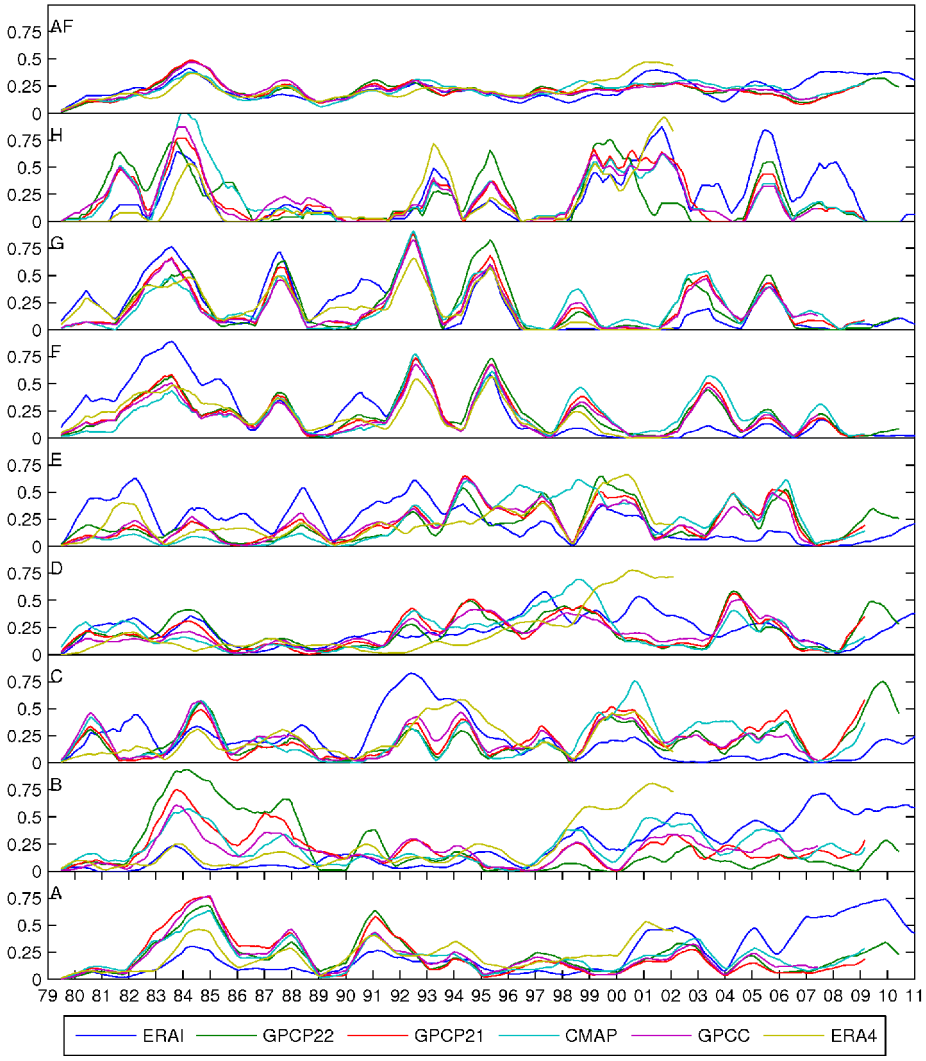

Figure 4. Time series of the fraction of each region (Table 1) in drought. Drought fraction is defined as the fraction of grid points with SPI12 bellow -0.8.

The time series of the fractional area of each region in drought, given by each precipitation dataset, is presented in Figure 4. The drought classification was based on SPI12, and represents the fraction of grid points of each area with a SPI12 < -0.8 in a particular time. The -0.8 threshold was initially defined by Svoboda et al. (2002) to quantify moderate droughts and has been used in other studies and applied to different standardized indices (e.g. Mo 2008). The fractional area in drought estimated from the different datasets highlights the large uncertainty in precipitation estimates that propagates into the drought index calculation. ERAI shows an increase of the fractional area in drought in regions A and B, that is associated with a drier model climate in the last decade, when compared with the 80s. This trend is also present in ERA-40, but not in the remaining datasets.

To further investigate the impact of the different precipitation datasets on SPI calculation, Figure 5a shows the correlation between SPI calculated with ERAI and GPCPv2.2 for 3, 6 and 12 months, as well as the monthly anomaly correlation between the two datasets. The regions with low correlations are mainly associated with the changes in ERAI precipitation climate. A detailed analysis if this feature of ERAI is beyond the scope of the present report, but a possible reason for this might be associated with changes in the satellite data entering the data assimilation system (also supported by a similar signal in ERA-40). When comparing the SPI calculated with ERAI with the previous version of GPCP v2.1 (Figure 5b) the correlations tend to be higher in all the time scales.

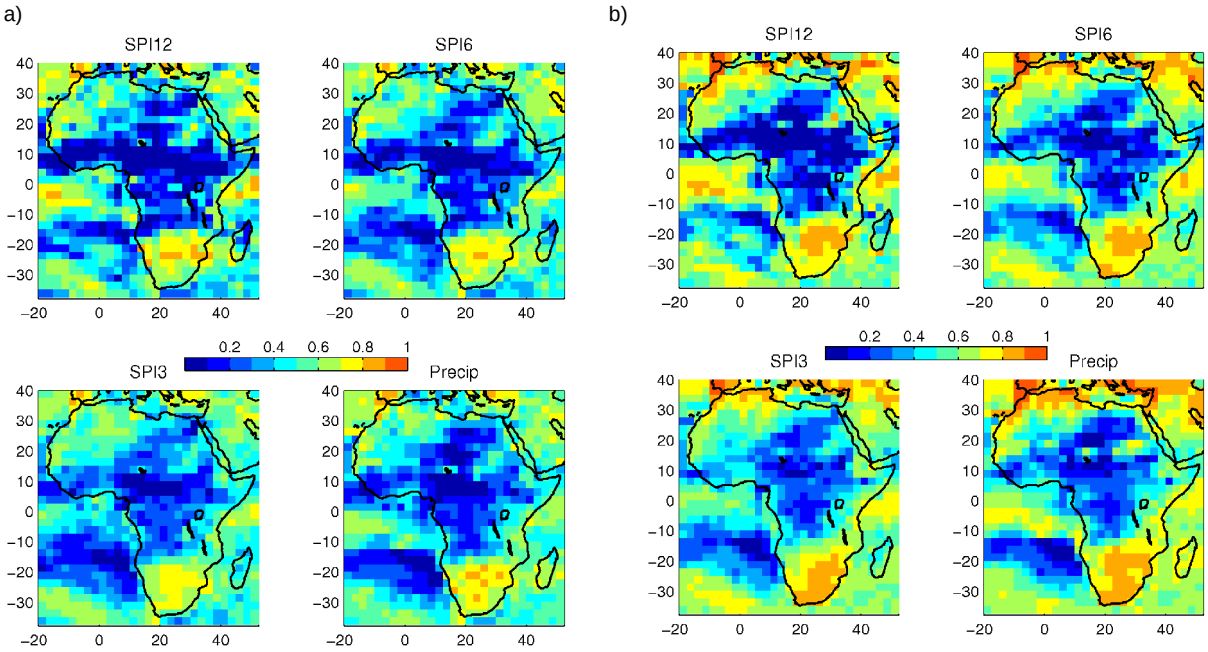

Figure 5. Grid point temporal correlation between ERA-Interim and GPCPv2.2 (a) and GPCPv2.1 (b) SPI12, SPI6, SPI3 and monthly precipitation (anomaly correlation).

2.3 SUMMARY

The comparison of four global precipitation datasets over Africa and ECMWF reanalysis highlight the uncertainty associated with accurate estimates of precipitation for verifying purposes. It was found that the use of ERAI precipitation has limitations, especially over the tropical rainforest, for drought applications due to changes in the model climate. However, in the other regions, it compares reasonably well with the remaining datasets and it has the potential to be used as a monitoring tool due to its near real time update (in contrast with the other datasets). Furthermore, a robust evaluation of seasonal forecasts is dependent on the verification dataset. Since there is no clear information on which dataset is more reliable, in the following chapter, the seasonal forecasts of precipitation will be verified against the new GPCP version (v2.2). These results highlight the uncertainty of precipitation estimates over Africa. Furthermore, a robust evaluation of seasonal forecasts is strongly dependent on the verification dataset. For example, Landman and Beraki (2010) verified seasonal forecasts of precipitation over southern Africa against the CRU dataset. In the next DEWFORA

deliverable, the seasonal forecasts of drought indexes will be verified against different datasets to assess the uncertainty of the verification due to selected verification dataset.

3. SEASONAL FORECASTS OF PRECIPITATION

Seasonal forecasting is the attempt to provide useful information about the "climate" that can be expected in the forthcoming coming months. The seasonal forecast is not strictly speaking a weather forecast: weather can be considered as a snapshot of continually changing atmospheric conditions, whereas climate is better considered as the statistical summary of the weather events occurring over a longer time period. Seasonal forecasts provide a range of possible climate changes that are likely to occur in the season ahead. It is important to bear in mind that, because of the chaotic nature of the atmospheric circulation, it is not possible to predict the daily weather variations at a specific location months in advance. It is not even possible to predict exactly the average weather, such as the average temperature for a given month.

In this chapter we present an evaluation of the skill of the seasonal forecasts of precipitation of four different systems and a multi-model composition.

3.1 DATA AND FORECAST SYSTEMS

The seasonal forecast systems were taken from the EUROSIP (EUROpean Seasonal to Inter-annual Prediction) archive at ECMWF. EUROSIP consists of 3 seasonal forecasting systems from ECMWF, Met Office and Météo-France (see Vitart et al.(2007) for further details). In addition to EUROSIP forecasts, we also evaluate the new ECMWF system 4, and a multi-model aggregation. The main characteristics of each system are listed in Table 2.

Table 2. Seasonal forecast systems

System name	Ensemble members	Hindcast period used	Horizontal Resolution
ECMWF system 3 **S3**	11	1981-2010	T159 (~1.125°)
ECMWF system 4 **S4**	15	1981-2010	T255 (~0.7°)
Météo-France system 3 **MF**	11	1981-2010	2.8°x2.8°
UK Met Office system 3 **UK**	15	1987-2008	2.5°x3.75° (lat/lon)
Multi-model **MM**	44 (4x11)	1987-2008	-

The ECMWF system 3 (S3) consists of Cy31r1 of the integrated forecast system (IFS) at TL159 resolution coupled with a 1° version of the HOPE ocean model. The IFS has 62 levels, extending up to approximately 5 hPa. Ocean initial conditions come from an assimilation system based on an advanced multivariate OI analysis with bias adjustments. Atmosphere and land surface initial conditions come from a mixture of ERA40 and ECMWF

operations. A more complete description is available in the ECMWF Seasonal Forecast User Guide[1].

The UK Met Office system (UK) as an atmospheric component with a spatial resolution of 2.5x3.75 deg grid. The ocean model has a basic resolution of 1.25 deg, but meridian refinement to 0.3 deg at the equator. Ocean initial conditions are taken from the Met Office ocean analysis system, including a fix to the ocean currents in the ocean initial conditions for start dates between May and October.

The Météo-France system (MF) is Arpege/ORCA. Arpege (the atmospheric component) has 91 vertical levels, reaching high into the stratosphere, and a spatial resolution of about 300Km. ORCA (the oceanic component) is an ocean model developed at LOCEAN in Paris. The ocean initial conditions are prepared by MERCATOR in Toulouse.

The ECMWF system 4 (S4) consists of the IFS model version 36r4. This model version was introduced for medium-range forecasting on 9th November 2010, although for seasonal forecasts a lower resolution is used: 91 levels in the vertical, with a model top in the mesosphere at 0.01 hPa, or a height of approximately 74 km. The spectral horizontal resolution used for seasonal forecasts is TL255. The ocean model used is NEMO, which replaces the HOPE ocean model used in S3. NEMO is used in the ORCA1 configuration, which has a 1x1 degree resolution in mid-latitudes and enhanced meridional resolution near the equator.

All seasonal forecast systems were interpolated (mass conserving) to the same 2.5°x2.5° grid that was used in the previous chapter. The multi-model (MM) results from the merging of the 11 ensemble members of each one of the four systems (S3, S4, MF, UK). For S4 and UK, the first 11 ensemble members were used, instead of the 15, to give an equal weight to each system in the multi-model. The merge was done after bias correcting each individual forecast.

Bias correction of each system was a necessary step to correct for model drift. Figure 6 displays the mean annual cycle of precipitation over Africa (see supplementary figures for the remaining regions) for each system and for each lead time. In this report, lead time one stands for the first month of forecast (date when the forecast was issued). The changes of the mean annual cycle with lead time in Figure 6 were corrected for each system (and for each calendar month and lead time) by a multiplicative factor calculated as the ratio between GPCPv2.2 and the mean of the hindcasts in each grid point.

[1] http://www.ecmwf.int/products/forecasts/seasonal/documentation/system3/

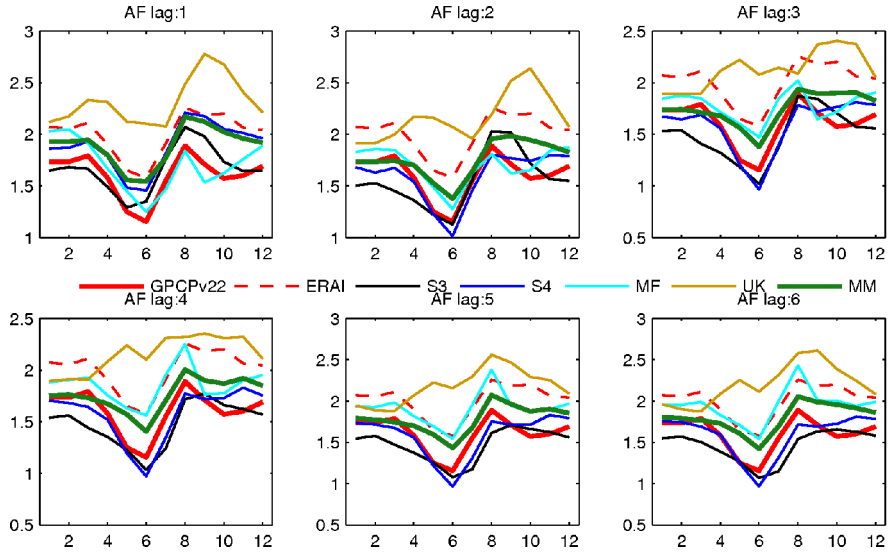

Figure 6. Comparison of the mean annual cycle of precipitation over Africa from GPCPv2.2 (red) and ERAI (dashed red) and seasonal forecasts of S3 (black), S4 (blue), MF (cyan), UK (brown) and MM (green). Each panel shows the mean annual cycle of the seasonal forecasts for a particular forecast lead time (1 to 6 months).

3.2 FORECASTS SKILL

The forecast skill of the different systems was evaluated in terms of the anomaly correlation coefficient (ACC) and the continuous rank probability skill score (CRPSS). The continuous rank probability score (CRPS, see Hersbach (2000) and references therein) is a development of the Ranked Probability Score. It can be also interpreted as the integral of the Brier score over all possible threshold values for the parameter under consideration. In deterministic forecasts, the CRPS reduces to the mean absolute error. Since the CRPS is not a normalized measure, we evaluate the CRPSS. For the skill score calculation the reference forecast is taken from GPCPv2.2 as a random sample of different years to produce a climatological forecast with the same ensemble size has the system that is verified.

We start by evaluating the skill of the forecasts over each region (Table 1), by averaging the precipitation from the bias corrected seasonal forecasts and GPCPv2.2 before the skill scores calculation. Figure 7 and Figure 8 display the ACC and CRPSS for each region as a function of initial forecast data for each calendar month and lead time. The evaluation is performed on 3 months average. For example, for the initial forecast month March, the lead time 3 represents the forecasts for May-July.

Although ACC is only based on the ensemble mean, and CRPSS accounts for the ensemble spread, both identify similar regions/ initial forecast data / lead time with and without skill. Regions A, B, C, F and G have several initial dates / lead time with skilful forecasts, while in regions D, E and H all the seasonal forecasts systems have difficulties in providing skilful forecasts. Comparing the different models, MF normally has the lower skill, while S3, S4 and UK share the best the skill in different regions. The multi-model composite (MM) tends to follow the best performing system.

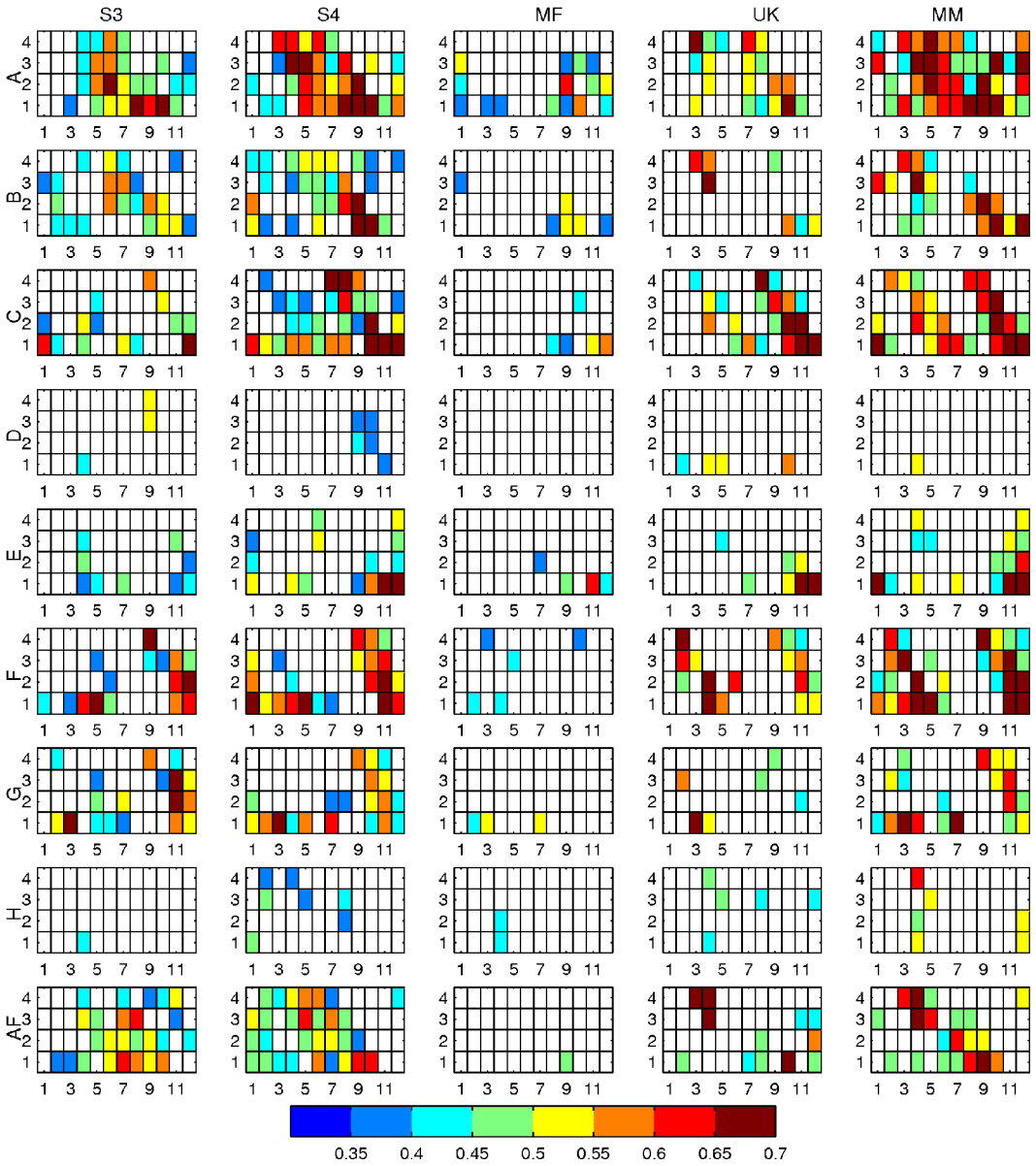

Figure 7. Anomaly correlation coefficient (ACC) of the seasonal forecasts of precipitation for each system (columns) in each region (lines). In each panel the horizontal axis represents the initial forecast month and the vertical axes the lead time. Each lead time represents 3-months averages. For example, for the initial forecast month March, the lead time 3 is the forecasts for May-July. Only correlations significant at 95% are coloured.

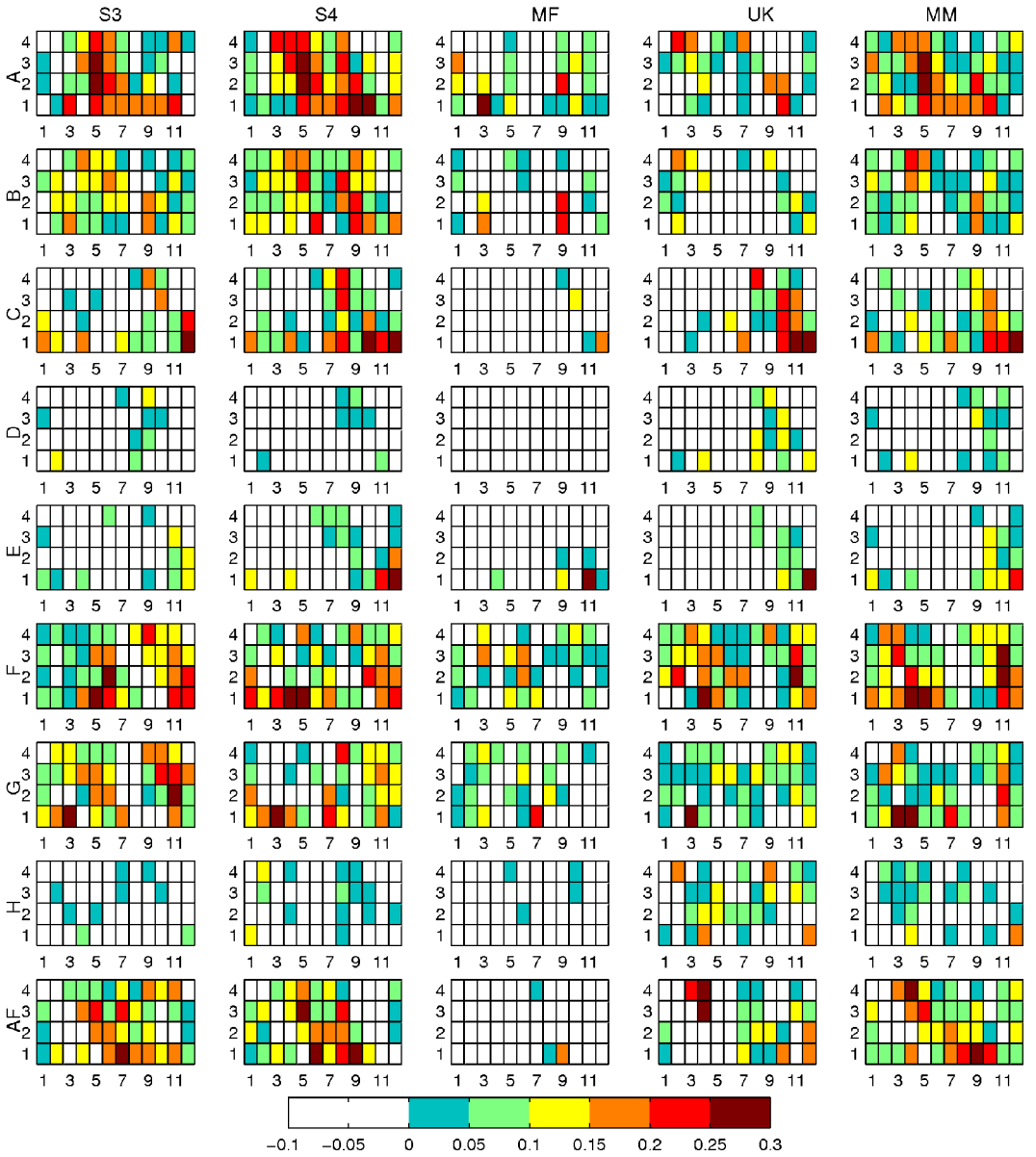

Figure 8. As Figure 7 but for the continuous rank probability skill score (CRPSS). Only CRPSS higher than zero are coloured.

Table 3 resumes the scores of each system for each region for time lag 2 (forecast months +2,+3 and +4). The MF system is consistently the worst system, followed by UK, while S3 and S4 are similar, although S4 tends to outperform S3. The MM tends to outperform the other systems, but this is not consistent for all regions, time lag and initial forecasts date. However, MM and S4 are similar, showing that most of the skill of the MM comes from S4. These preliminary results show that S4 can be used in detriment of the multi-model approach that is affected by a number of operational problems (see section 3.3).

Table 3. ACC and CRPSS for time lag 2 (forecast months +2,+3,+4) averaged for the 12 calendar months for each region. The numbers in brackets count the number of months (out of 12) where a specific system was the best. The bold numbers highlight the two systems with highest ACC and CRPSS in each region.

	ACC					CRPSS				
	S3	**S4**	**MF**	**UK**	**MM**	**S3**	**S4**	**MF**	**UK**	**MM**
A	0.41(1)	***0.45***(2)	0.23(2)	0.33(1)	**0.52**(6)	0.07(3)	**0.11**(3)	0.01(4)	-0.03(1)	**0.11**(1)
B	**0.37**(3)	**0.37**(3)	0.12(0)	0.25(0)	**0.41**(6)	**0.07**(5)	**0.08**(4)	-0.09(1)	-0.24(2)	0.04(0)
C	0.26(0)	**0.40**(6)	0.09(0)	0.29(1)	**0.42**(5)	-0.02(3)	**0.02**(4)	-0.22(0)	-0.08(3)	**0.03**(2)
D	**0.06**(1)	**0.06**(5)	-0.14(2)	0.1(3)	-0.02(1)	-0.17(4)	-0.24(1)	-0.65(0)	-0.23(5)	-0.19(2)
E	0.12(2)	**0.25**(4)	0.15(1)	0.22(3)	**0.29**(2)	-0.22(2)	-0.2(2)	-0.35(1)	-0.25(3)	-0.14(4)
F	0.24(1)	0.35(3)	0.09(0)	**0.36**(3)	**0.38**(5)	0.07(3)	0.06(2)	0. (0)	**0.1**(3)	**0.08**(4)
G	0.26(4)	**0.35**(5)	-0.03(0)	0.19(1)	**0.33**(2)	**0.05**(5)	**0.04**(5)	-0.04(2)	0.02(0)	**0.04**(0)
H	0.04(0)	0.16(2)	0.05(0)	**0.18**(6)	**0.19**(4)	-0.08(0)	-0.05(2)	-0.18(0)	**0.02**(8)	-0.04(2)
AF	0.32(3)	**0.33**(4)	0 (0)	0.25(1)	**0.33**(4)	0 (2)	**0.03**(4)	-0.30(0)	-0.09(1)	**0.04**(5)

As an example of a possible analysis we now focus on region G (Limpopo basin) for the forecasts valid to December-February (the peak rainy season). The spatial maps of ACC and CRPSS for the forecasts starting in November are displayed in Figure 9 and Figure 10, respectively (see supplementary figures for the remaining skill maps). For this particular region, lead time and initial forecast date, S3, S4, UK and MM can provide a skilful forecast. Furthermore, S4 provides skilful forecasts for Dec-Feb from September onwards.

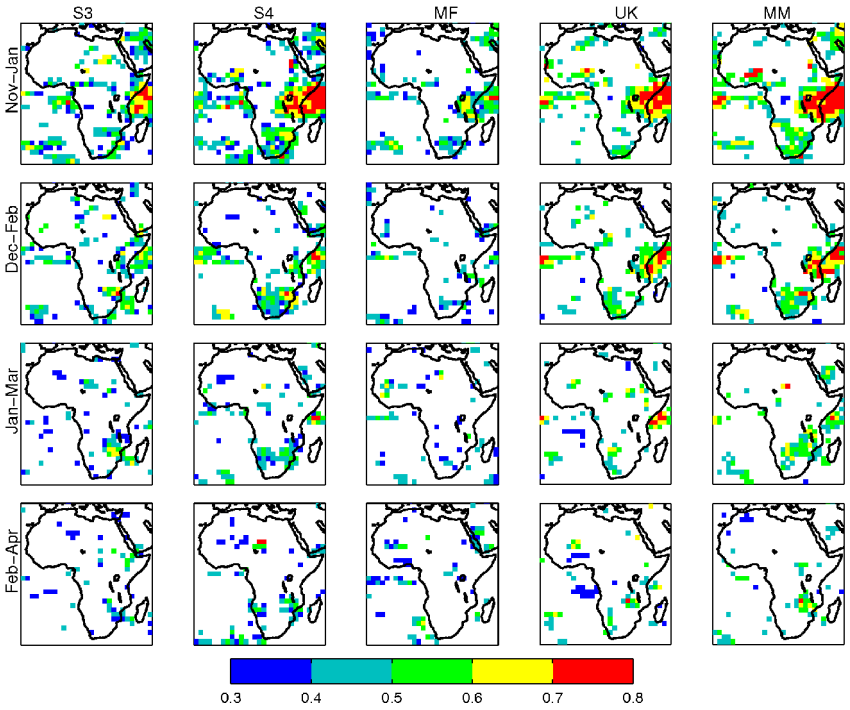

Figure 9. Anomaly correlations of the different seasonal forecasts (columns) starting in November for different lead times (lines) (3 months averages). Only correlations significant at 95% are represented.

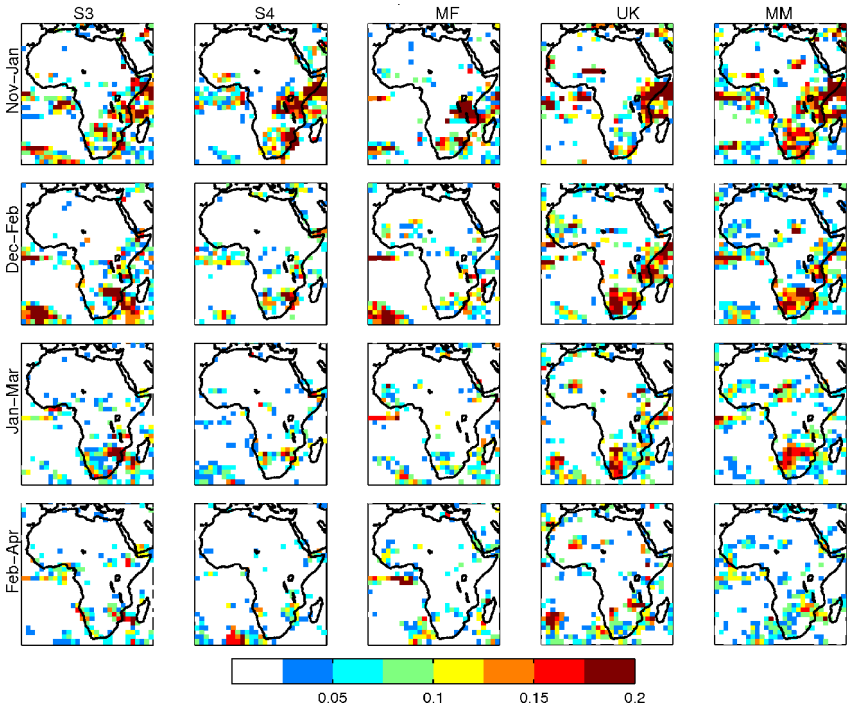

Figure 10. CRPSS of the different seasonal forecasts (columns) starting in November for different lead times (lines) (3 months averages). Only CRPSS higher than zero are represented.

3.3 SUMMARY

Forecast skill is usually highest when considering multi-model ensemble (MME) forecasts, created by combining forecasts from several different models. As an example of achievable skill, the MME forecast from the European DEMETER (Development of a European Multimodel Ensemble system for seasonal to inTERannual prediction) project (Palmer et al. 2004) has a anomaly correlation skill of 0.89 for 3-month lead prediction of the seasonally averaged NINO3.4 SST anomaly, with almost all the single coupled models' ACCs over 0.8, when assessed using hindcasts for the period 1980–2001. Landman and Beraki (2010) accessed the skill of mid-summer rainfall over southern Africa considering multi-model ensembles of downscaled forecasts from three of the DEMETER models. They found that the multi-model forecasts outperform the single forecasts and that the forecasts perform better during El Nino and La Nina season than during neutral years. Jin et al. (2008) created a larger ensemble by including 3 additional models from the Asia Pacific Economic Cooperation Climate Center (APCC) Climate Prediction and its Societal Application (CliPAS) project, giving a total of 10 models. They show that the MME again outperforms all of the individual models. In this report the MME (MM) performance does not consistently outperform a particular model. Although this could seem inconsistent with some literature, in this case the MME is a composite of only 4 systems, while most of the MME works combine more systems. Furthermore, S3 will be discontinued during 2012 and the UK system used in this report is an older version of the current system in operations. We did not include the current operational UK system due to the reduced number of hindcast years available at the

present. For these reasons, S4 from ECMWF is the best suitable seasonal forecast system to be used in DEWFORA.

Predictability in these coupled atmosphere-ocean systems comes mostly from large scale forcings. Region H (proxy for the Oum-er-Rbia Basin) has an almost constant rain of 1 mm day $^{-1}$ (usually near the threshold to set rain/no rain status), since the models do not represent most of the orographic induced rainfall in the region due to the coarser resolution. On the other hand, the other regions are affected by the West and East Africa monsoons that are associated with large scale forcings. These results highlight the importance and possible added value of statistical downscaling of the seasonal forecasts that might be able to capture large scale signals that are not present in the precipitation forecasts.

This report is not intended to present an extensive analysis on each case study area for the important lead times and forecast dates. Such analysis will be produced in detail within each case study considering not only the raw dynamical seasonal forecasts, but also statistical downscaling. Furthermore, this report is mainly focused on precipitation, while seasonal forecasts of derived drought indices, such as the SPI, will be evaluated and reported in future reports.

4. 2010-11 DROUGHT IN THE HORN OF AFRICA

It is estimated that the recent 2010-11 drought in the HoA affected approximately 12 million people. The drought in the region was the worst in the last 60 years (Loewenberg 2011). Although the main trigger of the crisis was the drought, other factors, including conflicts, population displacement and an increase in food and fuel prices led to a serious humanitarian crisis [http://reliefweb.int/horn-africa-crisis2011]. Although the HoA is not part of the DEWFORA case studies, it was decided to analyse and document this recent drought due to its social-economical impact, and as a demonstration of the potential outcome of DEWFORA in terms of tools and methodologies for drought monitoring and forecasting.

This chapter presents an evaluation of the ECMWF products in monitoring and forecasting drought conditions in the recent 2010-11 event in the HoA. The monitoring of the drought is evaluated through a comparison of the ERA-Interim reanalysis (ERAI, Dee et al. 2011) precipitation against several global datasets based on observations. Soil moisture, widely used as a drought indicator since it integrates precipitation anomalies in time (e.g. Dutra et al. 2008; Sheffield and Wood 2008), is also evaluated through the ERAI soil moisture anomalies. The precipitation anomalies of ERAI over the HoA are also examined in terms of teleconnection with the El Niño-Southern Oscillation (ENSO). The drought forecasts were evaluated by analyzing the skill of the ECMWF seasonal forecasts of El Niño and precipitation in the HoA during the 2010-11 wet seasons.

4.1 MONITORING

In this chapter the HoA region is defined as the land area between 3°S to 12° and 40°E to 52°E (see box in Figure 12), including Somalia, central and south Eastern Ethiopia (East of the Ethiopian Highlands) and a narrow band (about 1°) of Eastern Kenya, accounting for approximately 1.2×10^6 km^2(similar to the HoA sub-region used by *Mariotti et al.*(2011)). This selection is a sub-region of area C (see Table 1). The precipitation in the HoA region is characterized by two rainy seasons, March-May with higher intensity (“long rains”) and a second of shorter duration in October-December (“short rains”).

In addition to the observational-based datasets described in section 2.1, we included the Climate Research Unit version 3.1 (CRU3.1, updated from Mitchell and Jones 2005) dataset in the following analysis. This dataset, is only based in rain-gauges (as GPCC). Along with ERAI, the ECMWF numerical weather prediction operational deterministic forecasts (hereafter OP) of precipitation were also included in the analysis.

The ERAI mean annual cycle of precipitation over the HoA is comparable with the observation-based global datasets and is also similar to the previous ECMWF reanalysis ERA40 (Uppala et al. 2005), (Figure 11). All the datasets agree on the onset and the end of the rainy seasons, but differ in their intensity. ERAI predicts the highest peak values in both

seasons, suggesting an overestimation of intensity in the reanalysis product (also seen in ERA40). The challenges of representing the mean annual cycle of precipitation in the HoA in atmospheric models is known (Mariotti et al. 2011). However, it should also be highlighted that the global observation-based precipitation products used for comparison displayed a large uncertainty in the representation of the mean annual cycle of precipitation (Table 4). As expected, GPCC and the two GPCP versions are very similar, since they share similar data over land. ERAI has a precipitation anomaly correlation of 0.71 to the mean of all non-reanalysis products (Pmean).

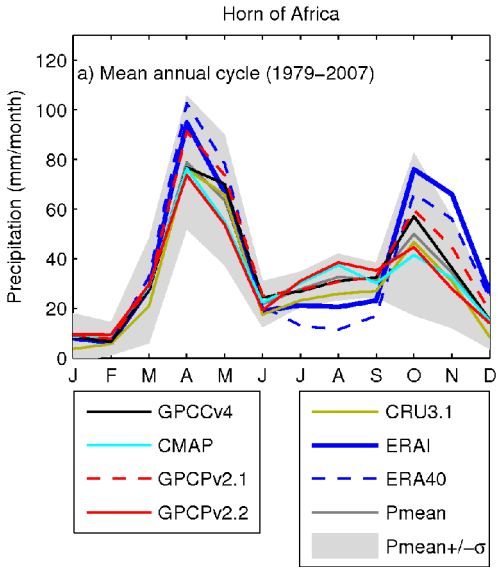

Figure 11. Mean annual cycle of the different precipitation products averaged over the HoA: GPCPv4 (black), CMAP (cyan), GPCPv2.1 (dashed red), GPCPv2.2 (solid red), CRU3.1 (brown), ERAI (thick blue), ERA40 (dashed blue, until 2001), Pmean (gray- mean of all the products except ERAI and ERA4), and the gray shading the Pmean +/- one standard deviation, representing the interannual variability. The mean annual cycle was calculated for the common period January 1979 to December 2007, while each dataset is available until: December 2007 (GPCCv4), September 2009 (CMAP, GPCPv2.1), December 2010 (GPCPv2.2) and December 2008 (CRU3.1).

Table 4. Anomaly correlations between the different monthly precipitation products averaged over the HoA for the common period 1979 to 2007 (2001 for ERA40). Pmean represents the mean of all products except ERAI and ERA40. All correlations are significant at 99%.

	ERA40	ERAI	CRU3.1	GPCCv4	CMAP	GPCPv2.1	GPCPv2.2	Pmean
ERA40	**1**	0.79	0.56	0.62	0.54	0.65	0.56	0.63
ERAI	0.79	**1**	0.55	0.70	0.62	0.74	0.65	0.71
CRU3.1	0.56	0.55	**1**	0.74	0.67	0.75	0.73	0.81
GPCCv4	0.62	0.70	0.74	**1**	0.81	0.98	0.95	0.98
CMAP	0.54	0.62	0.67	0.81	**1**	0.82	0.81	0.90
GPCPv2.1	0.65	0.74	0.75	0.98	0.92	**1**	0.96	0.98
GPCPv2.2	0.56	0.65	0.73	0.95	0.81	0.96	**1**	0.97
Pmean	0.63	0.71	0.81	0.98	0.90	0.98	0.97	**1**

Both ERAI and OP captured a strong precipitation anomaly in both rainy seasons (Figure 12). The Oct-Dec 2010 anomaly is also present in GPCPv2.2, and extends from the Western

Indian Ocean to the HoA, as in ERAI. The Mar-May 2011 anomaly had a smaller spatial extent and was mainly localized in the southern HoA. Notably, the accumulated precipitation from Sep 2010 to Aug 2011 in the HoA was the lowest of the ERAI 32 year record.

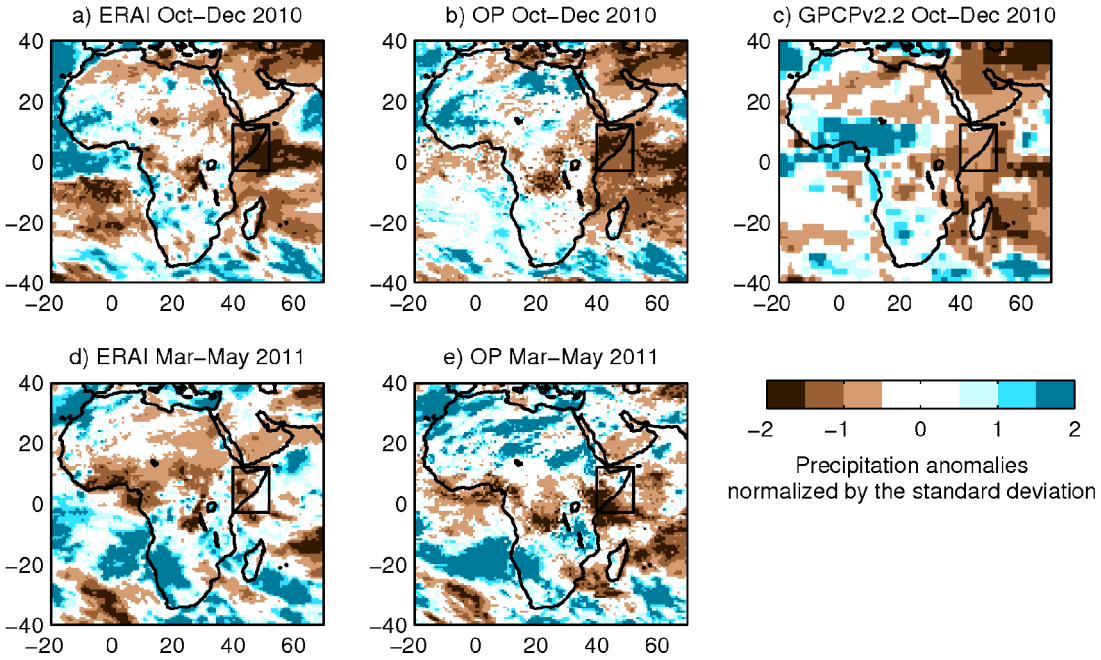

Figure 12. Spatial patterns of the precipitation anomalies normalized by the standard deviation (1979-2008) of Oct-Dec 2010 in ERAI (a), OP(b) and GPCPv2.2 (c) and of Mar-May 2011 in ERAI (d) and OP (e).

The temporal evolution of the reanalysis anomalies of precipitation and soil moisture from Jan 2010 to Sep 2011 indicates a severe drought situation in late 2010 to early 2011 (Figure 13). Mar-May 2010 was wetter than normal, while the Oct-Dec 2010 precipitation was below normal in both ERAI and GPCPv2.2. These results are consistent with the reported anomalies in the state of climate in 2010 (Blunden et al. 2011). The soil moisture in the top meter (Figure 13c) represents water availability to vegetation/crops (root zone), essential in the HoA region because of reliance on traditional rainfed agriculture (Haile 2005). The top meter soil moisture in ERAI started in an anomalous dry condition early in Oct 2010 and continued below the 10th percentile until Sep 2011. The full column soil moisture can be interpreted as an indicator of the long term water reservoirs, which suffered a strong depletion in 2011 after the two consecutive dry rain seasons. The full water column soil moisture anomaly in ERAI (Figure 13d) had a delayed drop below the 10th percentile in Nov 2010 and the dry departure from normal conditions it still evident in Sep 2011. The spatial patterns of the soil moisture anomalies are similar to the precipitation deficit patterns during Oct-Dec 2010 (Figure 14). However, during Mar-May 2011 the patterns of soil moisture anomalies show a wider spatial spread than that for the precipitation anomalies. These results highlight the role the soil moisture in monitoring droughts associated with the temporal integration of precipitation (forcing) and evaporation (demand) anomalies.

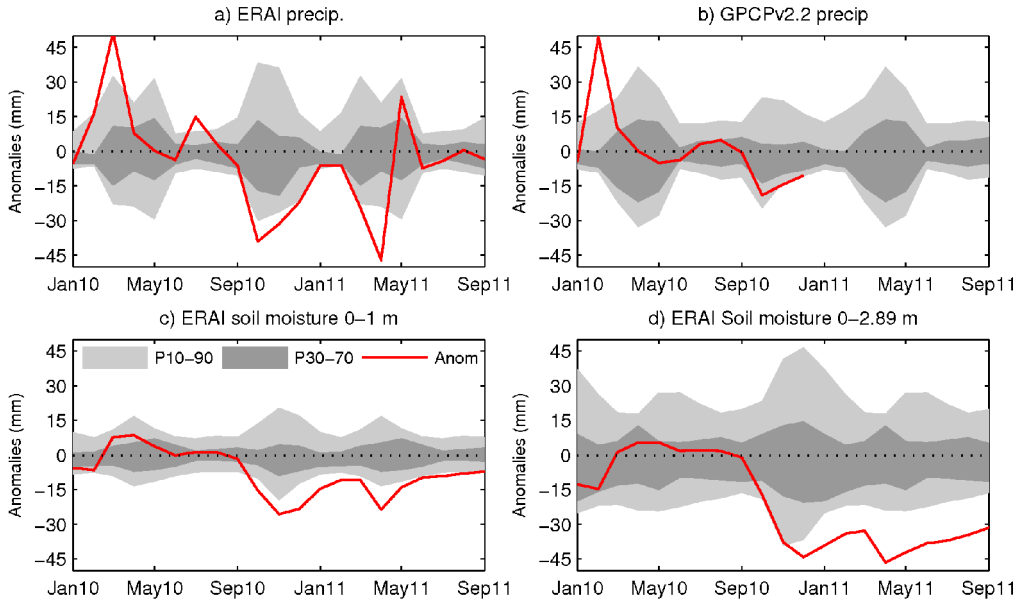

Figure 13. 2010-11 anomalies of precipitation from ERAI (a) and GPCPv2.2 (b), and ERAI soil moisture 0-1 m (c) and 0-2.89 m (d). The time series represent averages in the HoA of the anomaly (in red) and the climatological distribution between percentiles 10 to 90 (light gray), and percentiles 30 to 70 (darker gray). Note that GPCPv2.2 (b) is only available until December 2010.

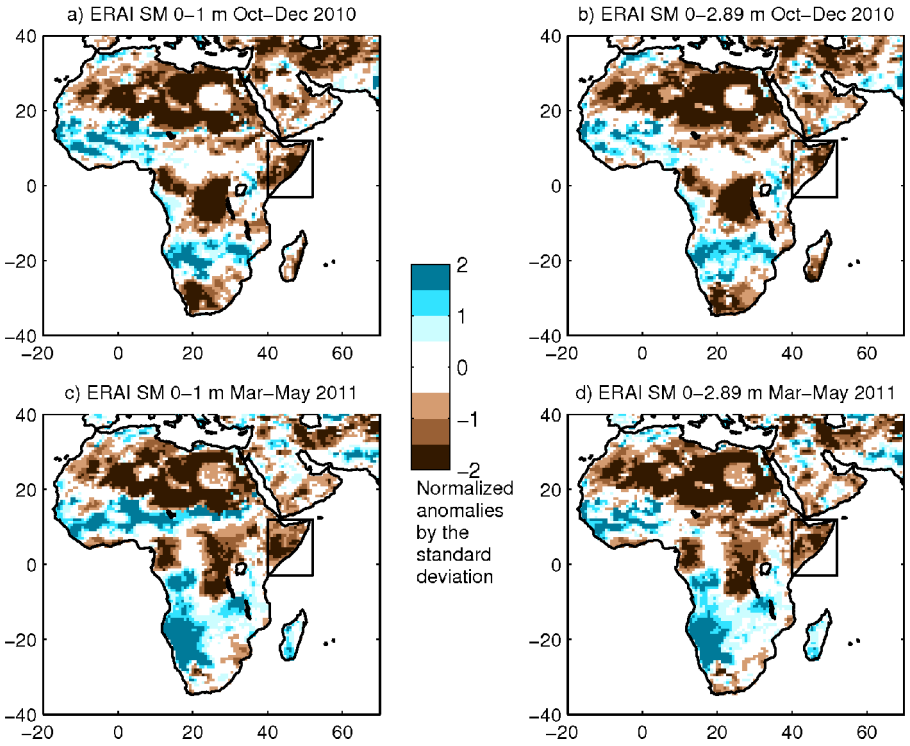

Figure 14. Spatial patterns of ERAI soil moisture normalized anomalies between 0-1 m deep (a, c) and 0-2.89 m (b, d) for Oct-Dec 2010 (a, b) and March-May 2011 (c, d).

4.2 ENSO TELECONNECTION AND SEASONAL FORECASTING

The teleconnection patterns between the HoA precipitation anomalies and the pacific sea surface temperature (SST) over the NINO3.4 region were evaluated to assess if there was evidence of large-scale forcing to the precipitation anomalies in 2010-11 (Figure 15a). The HoA precipitation versus NINO3.4 anomaly correlation is very similar between ERAI and

GPCP, indicating that the teleconnection with NINO3.4 is not an artefact of the analysis system. The highest correlations (~0.6) are found in the Oct-Dec season, while in the Mar-May season the correlations are close to zero. Comparing the Oct-Dec NINO3.4 against HoA precipitation anomaly illustrates this relation (Figure 15b), with positive precipitation anomalies during El Niño years (1997 strongest since 1979) and negative precipitation anomalies during La Niña years (1988 strongest and 2010 second strongest since 1979). This teleconnection pattern is also present in S3 (Figure 15c). The regression patterns of the Oct-Dec NINO3.4 against precipitation (Figure 16) further illustrate this teleconnection pattern showing that during La Niña years there is a negative precipitation anomaly centered over the western Indian Ocean, extending to East Africa. This teleconnection pattern is documented in other studies (e.g. Mutai and Ward 2000; Wolff et al. 2011), showing that an ENSO-forced weakening of the equatorial Walker-type cell, which is found over the Indian Ocean during the Oct-Dec season, is responsible for the abnormal wet rainfall anomalies in East Africa (Camberlin et al. 2001).

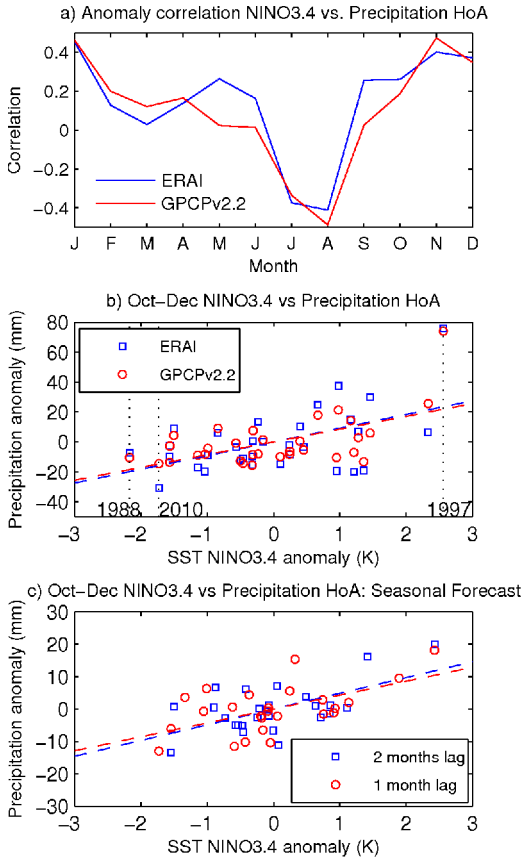

Figure 15. a) Anomaly correlation between NINO3.4 and precipitation in the Horn of Africa from ERAI (blue) and GPCPCv2.2 (red). The anomaly correlations were calculated using a three months moving window. b) Mean October to December precipitation anomalies from ERAI (blue) and GPCPv2.2 (red) as a function of NINO3.4. The two strongest La-Nina events (1988 and 2010) and the strongest El-Nino event (1997) are highlighted with vertical dashed lines. c) as b) but for the seasonal forecasts valid at Oct-Dec starting in August (2 months lag, blue points), and September (1 month lag, red points). In panels b) and c) the dashed lines represent a linear regression between NINO3.4 and precipitation anomalies with

slopes (+/- 95% confidence interval): b) ERAI: 9.2 +/-5.6; GPCP: 8.6 +/- 4.5; c) 2 months lag: 4.9 +/- 2.8; 1 month lag: 4.3 +/-2.7 mm K^{-1}.

a) Regression ERAI precipitation on NINO3.4 Oct-Dec

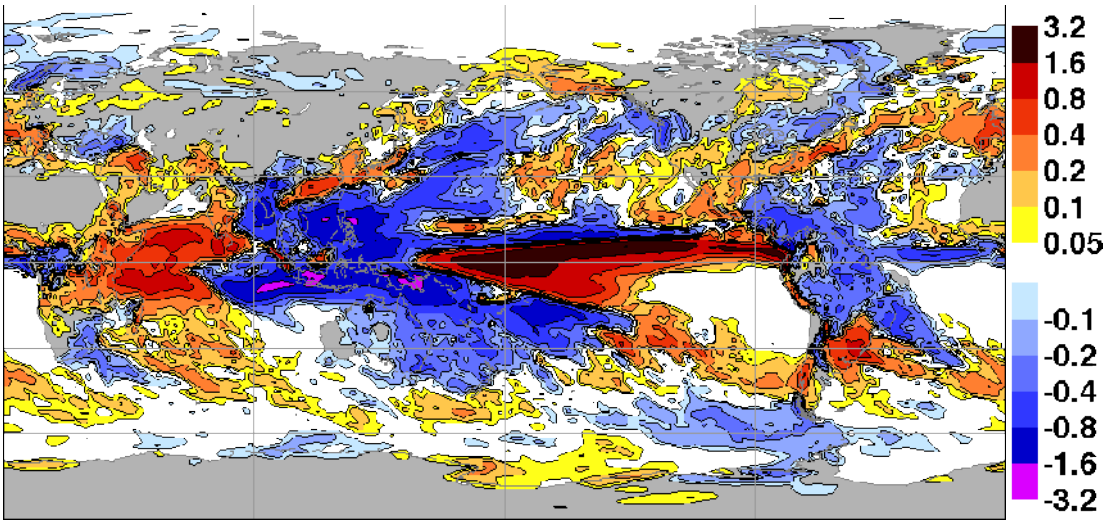

b) Regression GPCP precipitation on NINO3.4 Oct-Dec

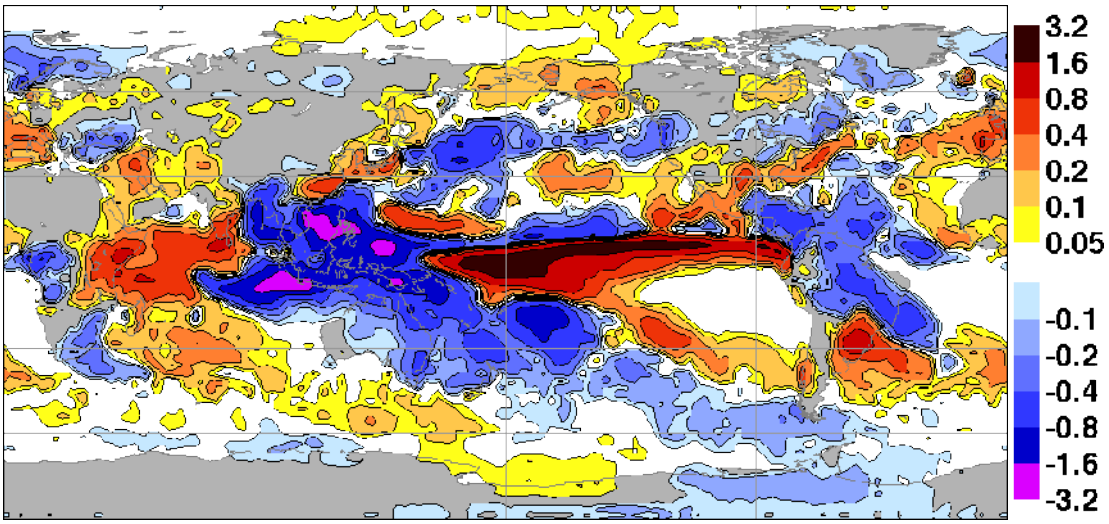

Figure 16. Linear regression patterns of ERAI (a) and GPCP (b) October to December precipitation on to NINO3.4 for the same period.

The Oct-Dec 2010 season was characterized by a strong cold anomaly in the sea surface temperature in the Pacific Ocean (La Niña) (Figure 17). This anomaly started early in June 2010 extending up to April 2011 with minimum values between Sep 2010 and Jan 2011. This La Niña event and its persistence were correctly forecasted by the ECMWF seasonal forecasts S3, from Jun/Jul 2010 onwards. The recovery to warmer (normal) conditions started in February 2011, and was also correctly captured by the seasonal forecasts. This is consistent with *Stockdale et al.*, (2011) who found a demonstrable skill in S3 in predicting El Niño variability. The seasonal forecasts of precipitation for the Oct-Dec 2010 season predicted a dry season from Jul 2010 onwards (Figure 18a). On the other hand, the 2011 Mar-May precipitation anomaly was not captured in advance by the seasonal forecast, except for the forecast started in Mar 2011.

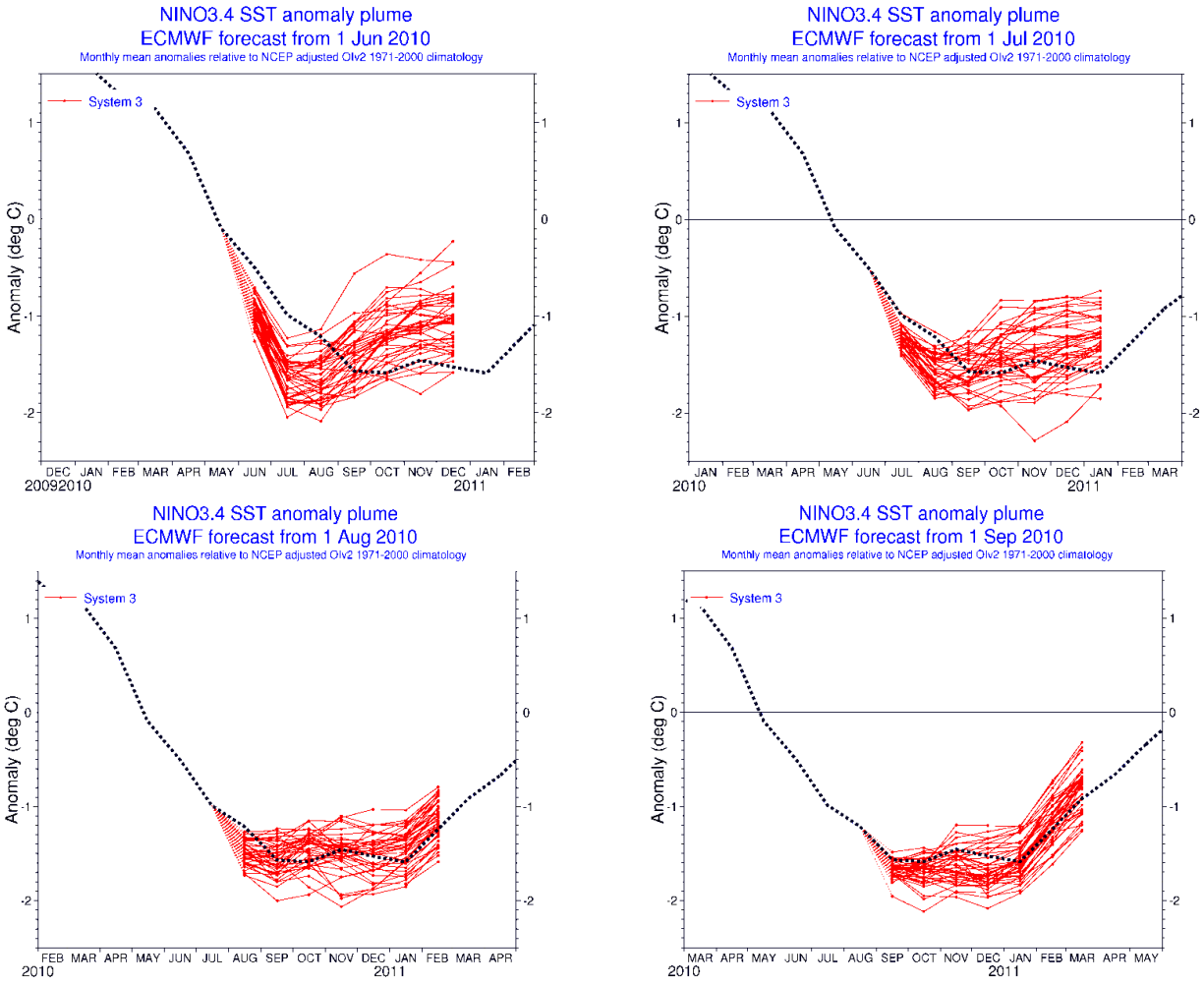

Figure 17. ECMWF ensemble seasonal forecasts (red) and observed (dashed black) NINO3.4 sea surface temperature anomalies in the NINO3.4 region for the forecasts starting in June to September 2010.

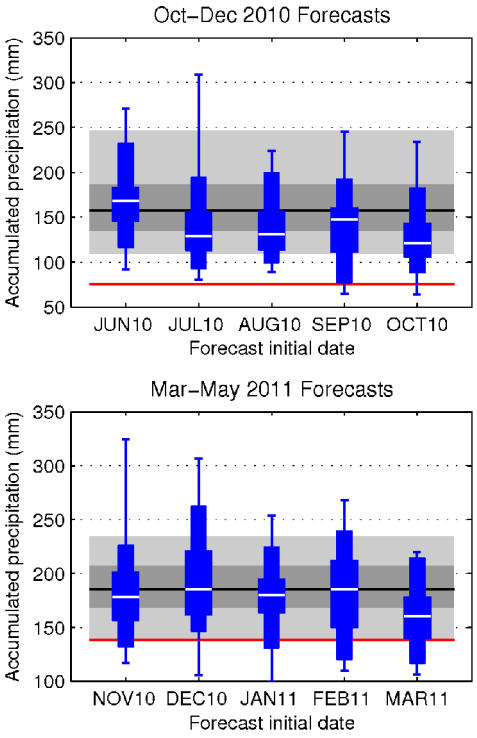

Figure 18. Distribution of the seasonal forecasts of precipitation for Oct-Dec 2010 (top) and Mar-May 2011 (bottom). The gray areas indicate the model climate distribution between percentiles 10 to 90 (light gray) and percentiles 30 to 70 (dark gray), with the median (black line). The horizontal axis represents the forecast initial date with one ensemble forecast for each month represented as boxplots extending from the minimum (whiskers), percentiles 10, 30, 50 (white line), 70, 90 and maximum. The red line in both panels represents the ERAI accumulated precipitation. The model climate was bias corrected to match ERAI.

4.3 SUMMARY

In this study, the use of ECMWF products were evaluated, in monitoring and forecasting drought conditions during the recent 2010-11 event in the Horn of Africa (HoA).

The ERAI precipitation anomalies compare well with other observation-based global datasets, noting that these datasets present a large uncertainty in the HoA. This is in line with the findings of *Shin et al.* (2011). The 2010-11 drought resulted from a precipitation deficit in both the Oct-Dec 2010 and Mar-May 2011 rainy seasons, and this was captured by ERAI. Soil moisture anomalies of ERAI also indentified the onset of the drought condition early in Oct 2010 with a persistent drought still present in Sep 2011.

The precipitation deficit in Oct-Dec 2010 was associated with a strong La Niña event. The ECMWF seasonal forecasts of NINO3.4 predicted the La Niña event from June 2010 onwards, and also a dry precipitation anomaly for the region from July 2010 onwards. On the other hand, the seasonal forecasts for the Mar-May 2011 season did not predict the anomaly in advance, except for the forecasts in March 2011. This is consistent with the findings of Camberlin and Philippon (2002) reporting that the Mar-May season does not exhibit strong relationships with any large-scale climate anomalies.

Climate scenarios for the 21th century suggest an average increase of precipitation in the HoA region (Mariotti et al. 2011; Paeth et al. 2009), that might result in a decrease of moderate droughts (Burke and Brown 2008) (a signal also found in soil moisture simulations for the present climate (Sheffield and Wood 2008)). However, there are also some indications of an increased variability of rainfall in the future (Wolff et al. 2011). Even with an increase of mean precipitation, the increase of interannual variability associated with social and political conflicts makes this region and its population highly vulnerable to future droughts, thus global monitoring and forecasting of drought, such as that presented here, is going to become increasingly important in the future.

5. REFERENCES

Blunden, J., D. S. Arndt, and M. O. Baringer, 2011: State of the Climate in 2010, *Bull. Amer. Meteor. Soc.*, **92**(6), S1-S236, doi: 10.1175/1520-0477-92.6.s1.

Burke, E. J., and S. J. Brown, 2008: Evaluating Uncertainties in the Projection of Future Drought, *J. Hydrometeor.*, **9**(2), 292-299, doi: 10.1175/2007jhm929.1.

Camberlin, P., S. Janicot, and I. Poccard, 2001: Seasonality and atmospheric dynamics of the teleconnection between African rainfall and tropical sea-surface temperature: Atlantic vs. ENSO, *Int. J. Climatol.*, **21**(8), 973-1005, doi: 10.1002/joc.673.

Camberlin, P., and N. Philippon, 2002: The East African March-May Rainy Season: Associated Atmospheric Dynamics and Predictability over the 1968-97 Period, *J. Climate*, **15**(9), 1002-1019, doi: 10.1175/1520-0442(2002)015<1002:teammr>2.0.co;2.

Cane, M. A., S. E. Zebiak, and S. C. Dolan, 1986: Experimental forecasts of El Nino, *Nature*, **321**(6073), 827-832.

Dee, D. P., and Coauthors, 2011: The ERA-Interim reanalysis: configuration and performance of the data assimilation system, *Quart. J. Roy. Meteor. Soc.*, **137**(656), 553-597, doi: 10.1002/qj.828.

Di Giuseppe, F., F. Molteni, and A. M. Tompkins, 2011: A rainfall calibration methodology for impact modelling based on spatial mapping, *Quart. J. Roy. Meteor. Soc.*, **submitted**.

Dutra, E., P. Viterbo, and P. M. A. Miranda, 2008: ERA-40 reanalysis hydrological applications in the characterization of regional drought, *Geophys. Res. Lett.*, **35**, L19402, doi:19410.11029/12008GL035381.

Fuchs, T., and e. al., 2009: GPCC annual report for yer 2008: Development of the GPCC data base and anaysis products., *Global Precipitation Climatology Centre*, 13 pp [available online at http://www.gpcc.dwd.de].

Haile, M., 2005: Weather patterns, food security and humanitarian response in sub-Saharan Africa, *Philosophical Transactions of the Royal Society B-Biological Sciences*, **360**(1463), 2169-2182, doi: 10.1098/rstb.2005.1746.

Hersbach, H., 2000: Decomposition of the Continuous Ranked Probability Score for Ensemble Prediction Systems, *Weather and Forecasting*, **15**(5), 559-570, doi: 10.1175/1520-0434(2000)015<0559:dotcrp>2.0.co;2.

Huffman, G. J., R. F. Adler, D. T. Bolvin, and G. Gu, 2009: Improving the global precipitation record: GPCP Version 2.1, *Geophys. Res. Lett.*, **36**(17), L17808, doi: 10.1029/2009gl040000.

Jin, E., and Coauthors, 2008: Current status of ENSO prediction skill in coupled ocean-atmosphere models, *Climate Dyn.*, **31**(6), 647-664, doi: 10.1007/s00382-008-0397-3.

Keyantash, J., and J. A. Dracup, 2002: The quantification of drought: An evaluation of drought indices, *Bull. Amer. Meteor. Soc.*, **83**(8), 1167-1180.

Landman, W. A., and A. Beraki, 2010: Multi-model forecast skill for mid-summer rainfall over southern Africa, *Int. J. Climatol.*, n/a-n/a, doi: 10.1002/joc.2273.

Loewenberg, S., 2011: Humanitarian response inadequate in Horn of Africa crisis, *The Lancet*, **378**(9791), 555-558.

Mariotti, L., E. Coppola, M. B. Sylla, F. Giorgi, and C. Piani, 2011: Regional climate model simulation of projected 21st century climate change over an all-Africa domain: Comparison analysis of nested and driving model results, *J. Geophys. Res.*, **116**(D15), D15111, doi: 10.1029/2010jd015068.

Mckee, T. B., N. J. Doesken, and J. Kleist, 1993: The relationship of drought frequency and duration to time scales. *Eight Conference on Applied Climatology*.

Mitchell, T. D., and P. D. Jones, 2005: An improved method of constructing a database of monthly climate observations and associated high-resolution grids, *Int. J. Climatol.*, **25**(6), 693-712.

Mo, K. C., 2008: Model-Based Drought Indices over the United States, *J. Hydrometeor.*, **9**(6), 1212-1230, doi: 10.1175/2008jhm1002.1.

Mutai, C. C., and M. N. Ward, 2000: East African Rainfall and the Tropical Circulation/Convection on Intraseasonal to Interannual Timescales, *J. Climate*, **13**(22), 3915-3939, doi: 10.1175/1520-0442(2000)013<3915:earatt>2.0.co;2.

Paeth, H., K. Born, R. Girmes, R. Podzun, and D. Jacob, 2009: Regional Climate Change in Tropical and Northern Africa due to Greenhouse Forcing and Land Use Changes, *J. Climate*, **22**(1), 114-132, doi: 10.1175/2008jcli2390.1.

Palmer, T. N., and Coauthors, 2004: DEVELOPMENT OF A EUROPEAN MULTIMODEL ENSEMBLE SYSTEM FOR SEASONAL-TO-INTERANNUAL PREDICTION (DEMETER), *Bull. Amer. Meteor. Soc.*, **85**(6), 853-872, doi: 10.1175/bams-85-6-853.

Sheffield, J., and E. F. Wood, 2008: Global Trends and Variability in Soil Moisture and Drought Characteristics, 1950–2000, from Observation-Driven Simulations of the Terrestrial Hydrologic Cycle, *J. Climate*, **21**(3), 432-458, doi: 10.1175/2007jcli1822.1.

Shin, D.-B., J.-H. Kim, and H.-J. Park, 2011: Agreement between monthly precipitation estimates from TRMM satellite, NCEP reanalysis, and merged gauge-satellite analysis, *J. Geophys. Res.*, **116**(D16), D16105, doi: 10.1029/2010jd015483.

Stockdale, T., and Coauthors, 2011: ECMWF seasonal forecast system 3 and its prediction of sea surface temperature, *Climate Dyn.*, **37**(3), 455-471, doi: 10.1007/s00382-010-0947-3.

Svoboda, M., and Coauthors, 2002: The Drought Monitor, *Bull. Amer. Meteor. Soc.*, **83**(8), 1181-1190, doi: 10.1175/1520-0477(2002)083<1181:tdm>2.3.co;2.

Uppala, S. M., and Coauthors, 2005: The ERA-40 re-analysis, *Quart. J. Roy. Meteor. Soc.*, **131**(612), 2961-3012, doi: 10.1256/qj.04.176.

Vitart, F., and Coauthors, 2007: Dynamically-based seasonal forecasts of Atlantic tropical storm activity issued in June by EUROSIP, *Geophys. Res. Lett.*, **34**(16), L16815, doi: 10.1029/2007gl030740.

WMO, 2009, **Press release, December 2009 No 872**.

Wolff, C., and Coauthors, 2011: Reduced Interannual Rainfall Variability in East Africa During the Last Ice Age, *Science*, **333**(6043), 743-747, doi: 10.1126/science.1203724.

Xie, P., and P. A. Arkin, 1997: Global Precipitation: A 17-Year Monthly Analysis Based on Gauge Observations, Satellite Estimates, and Numerical Model Outputs, *Bull. Amer. Meteor. Soc.*, **78**(11), 2539-2558, doi: 10.1175/1520-0477(1997)078<2539:gpayma>2.0.co;2.

6. SUPPLEMENTARY FIGURES

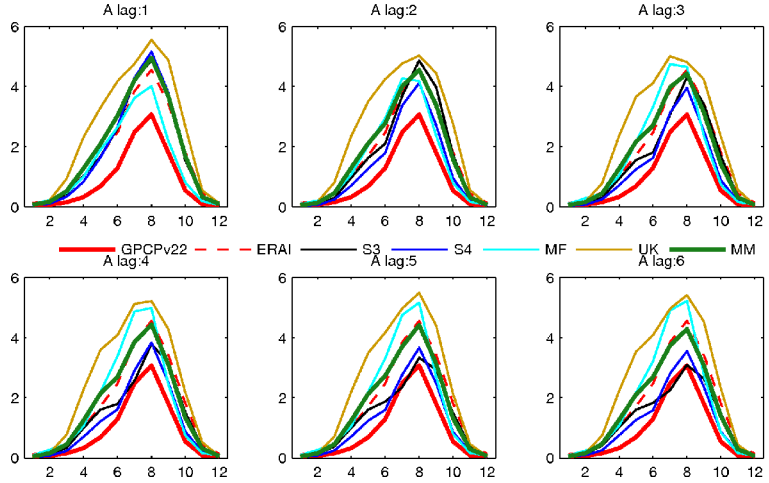

Figure 19. As Figure 6 but for region A.

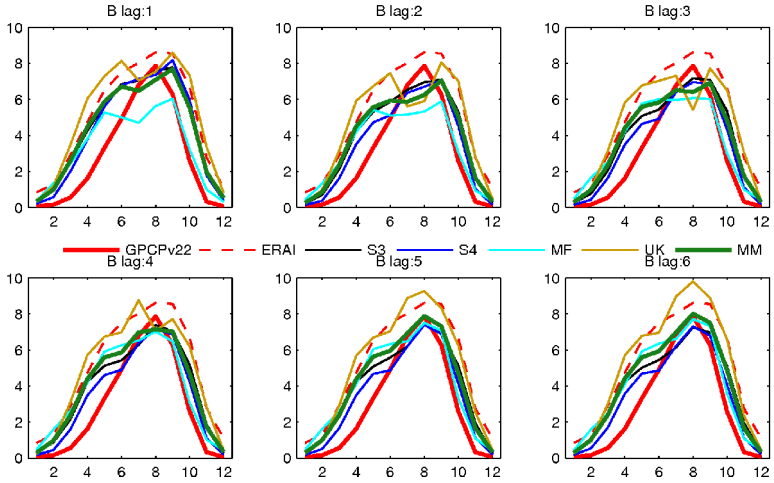

Figure 20. As Figure 6 but for region B.

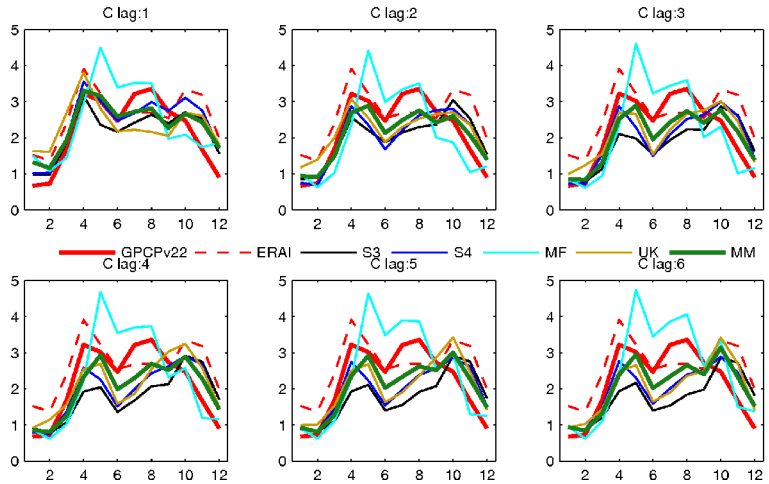

Figure 21. As Figure 6 but for region C.

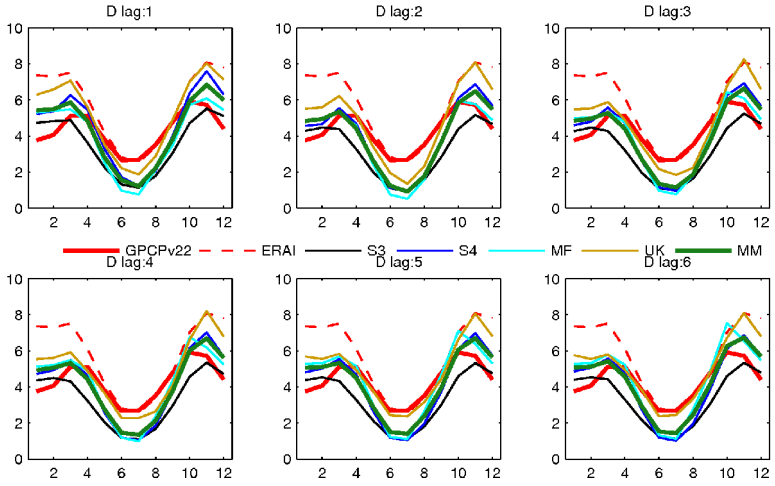

Figure 22. As Figure 6 but for region D.

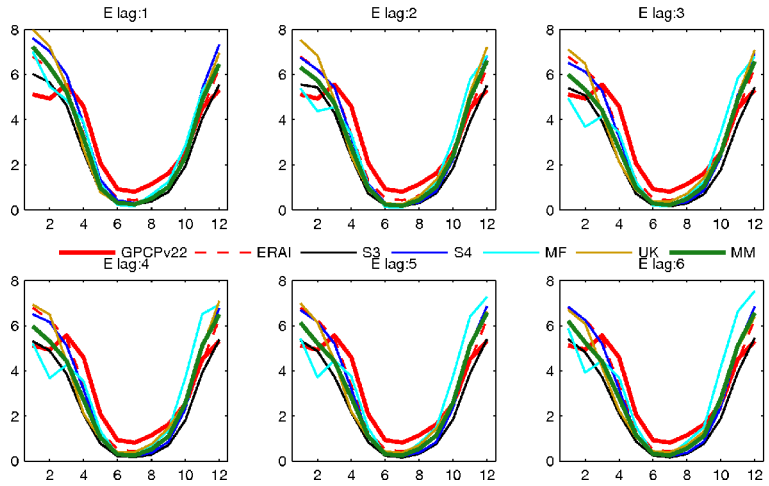

Figure 23. As Figure 6 but for region E.

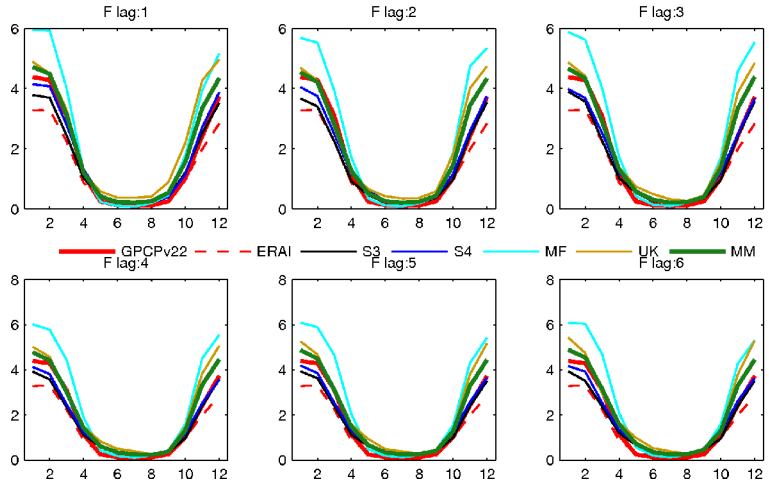

Figure 24. As Figure 6 but for region F.

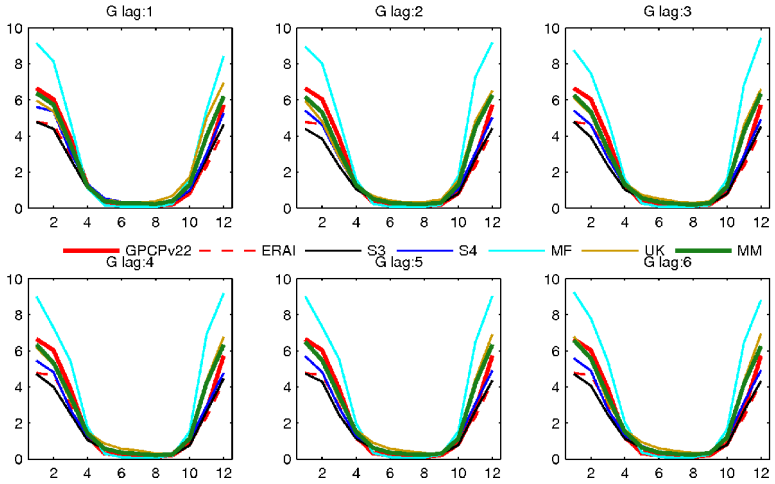

Figure 25. As Figure 6 but for region G.

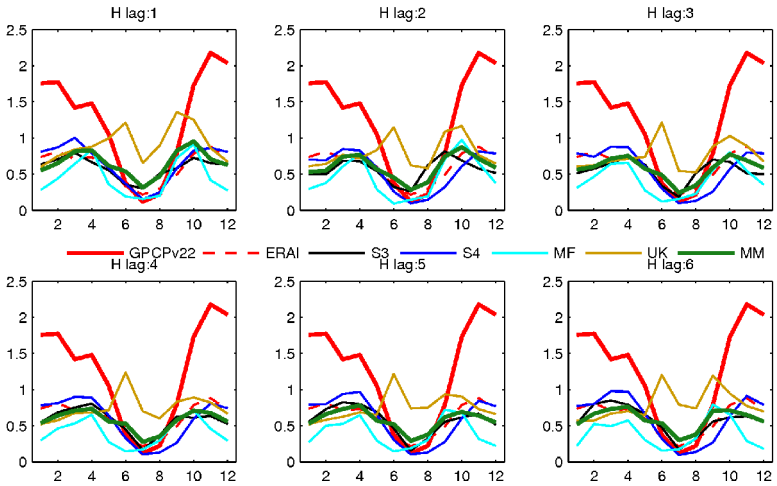

Figure 26. As Figure 6 but for region H.

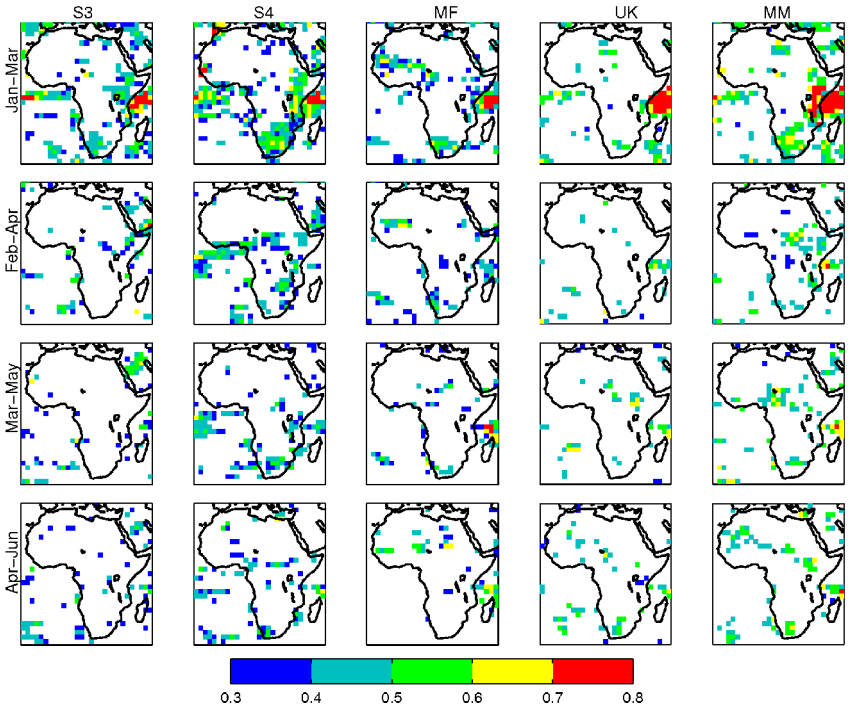

Figure 27. As Figure 9 but for the forecasts starting in January.

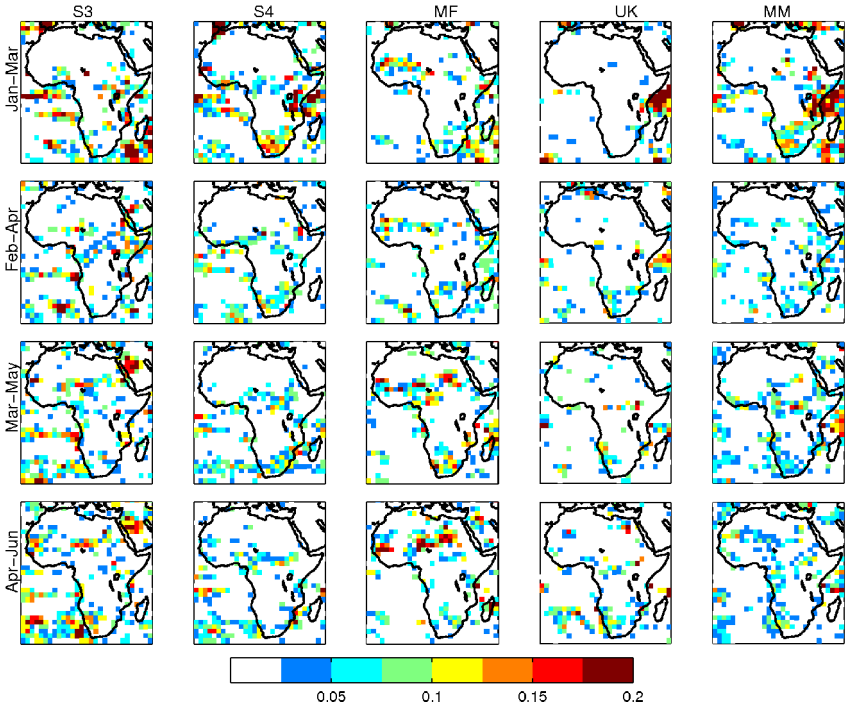

Figure 28. As Figure 10 but for the forecasts starting in January.

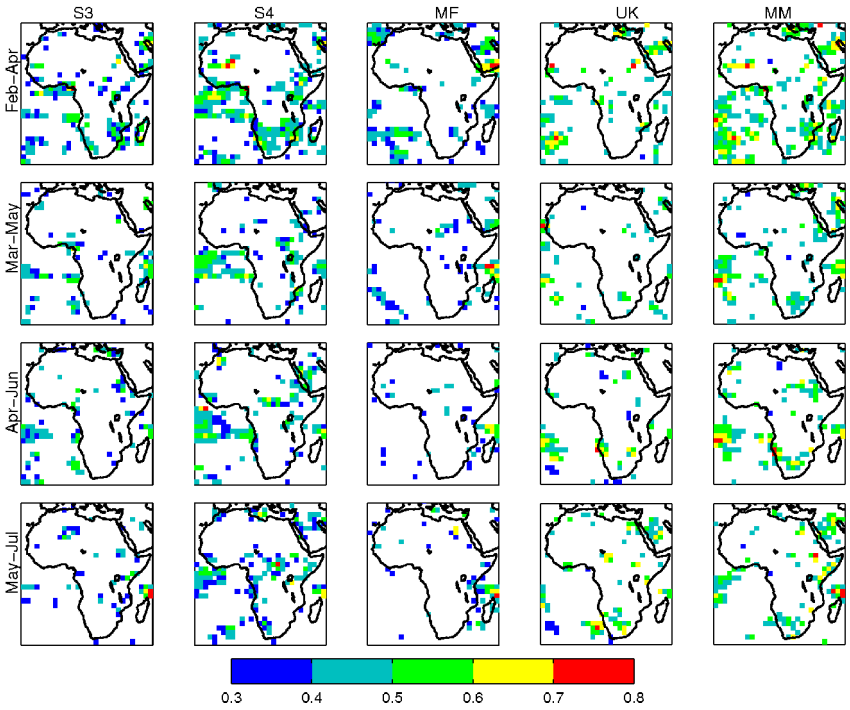

Figure 29. As Figure 9 but for the forecasts starting in February.

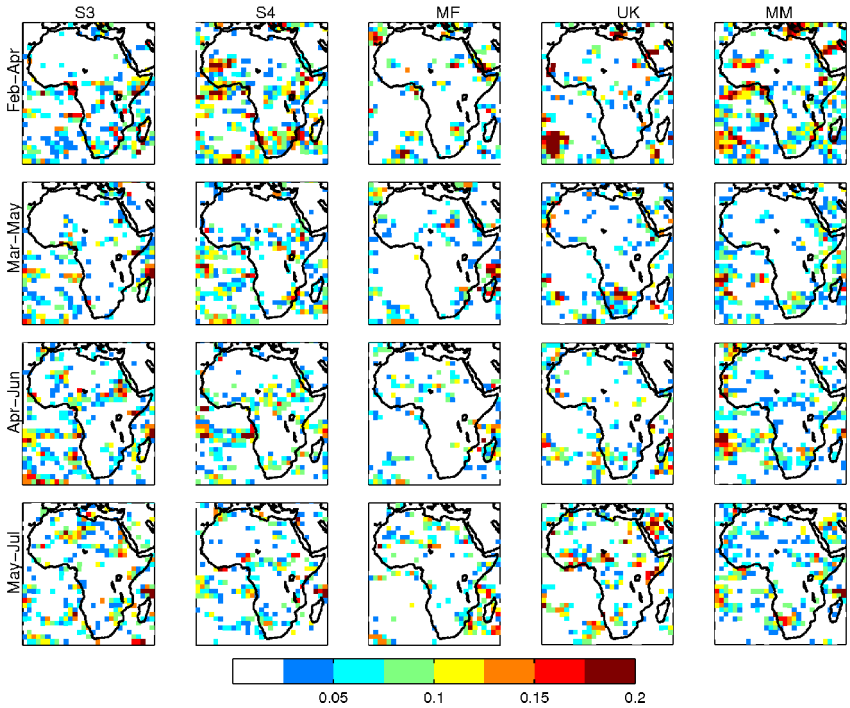

Figure 30. As Figure 10 but for the forecasts starting in February.

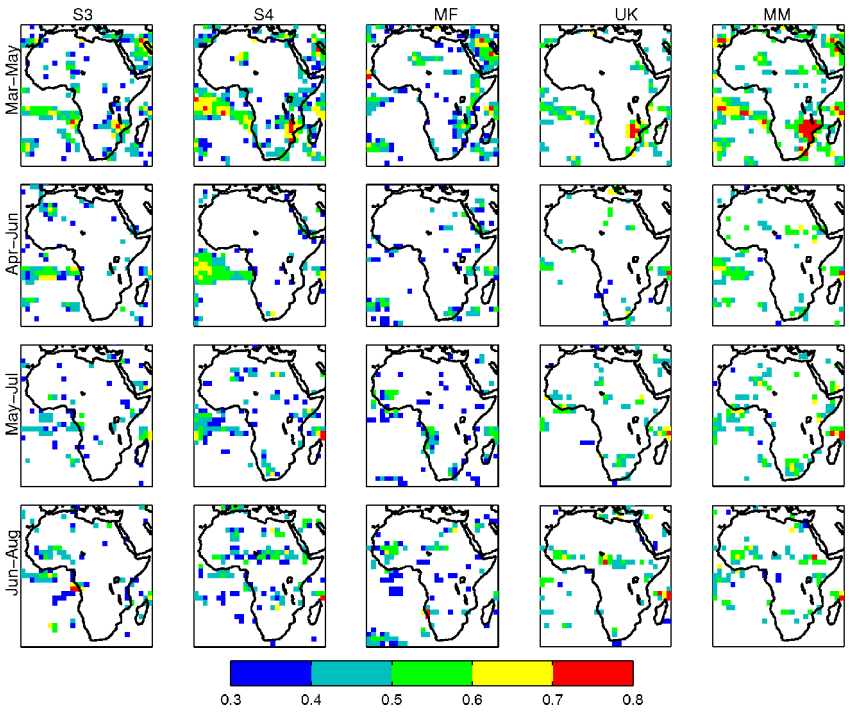

Figure 31. As Figure 9 but for the forecasts starting in March.

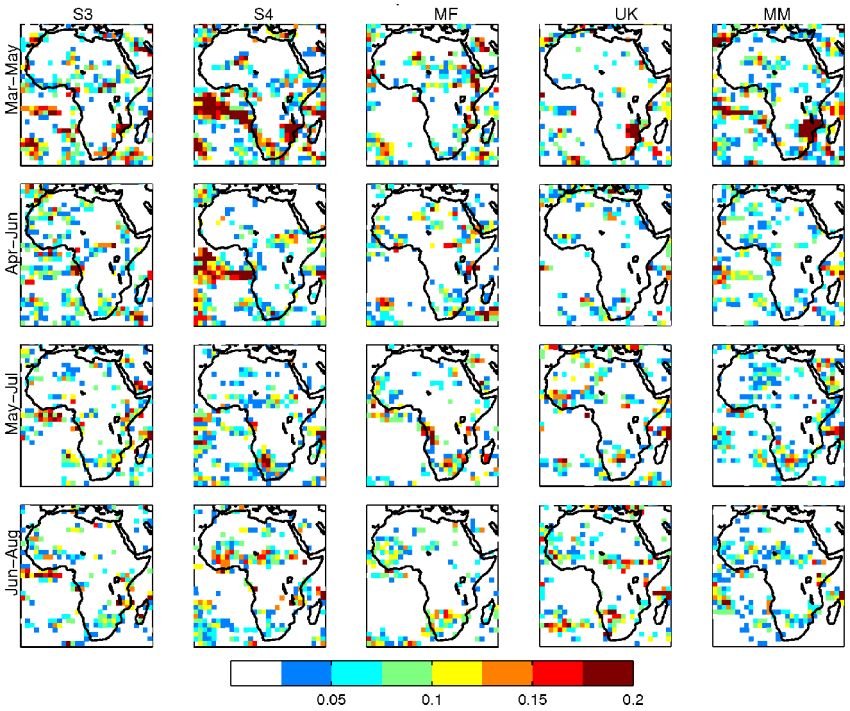

Figure 32. As Figure 10 but for the forecasts starting in March.

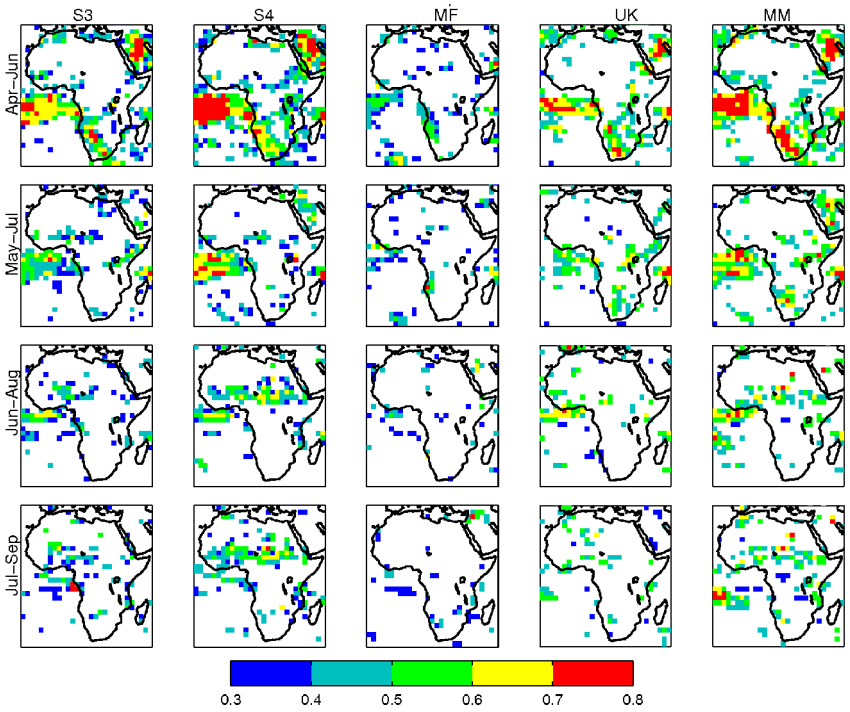

Figure 33. As Figure 9 but for the forecasts starting in April.

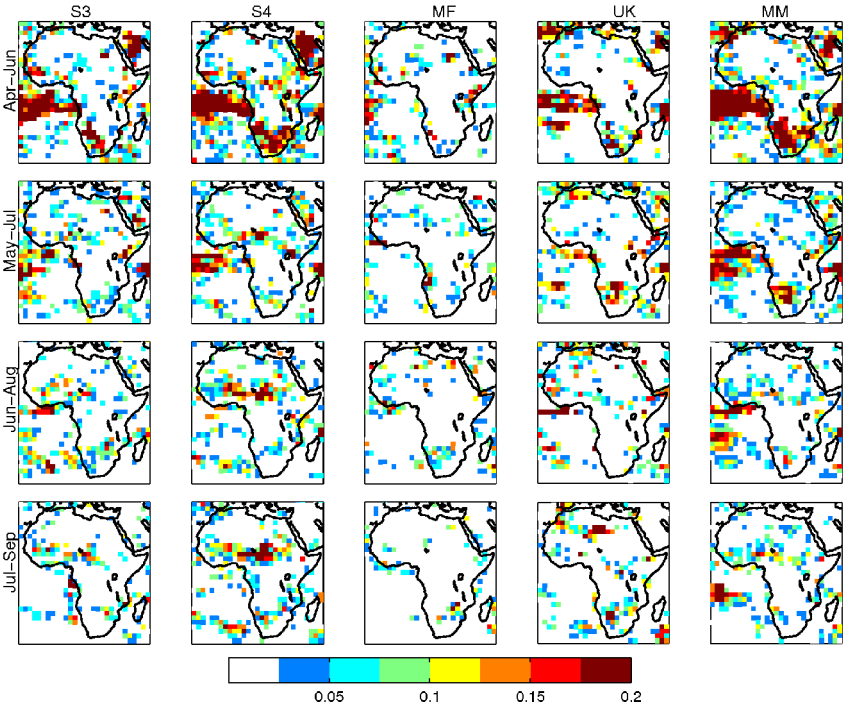

Figure 34. As Figure 10 but for the forecasts starting in April.

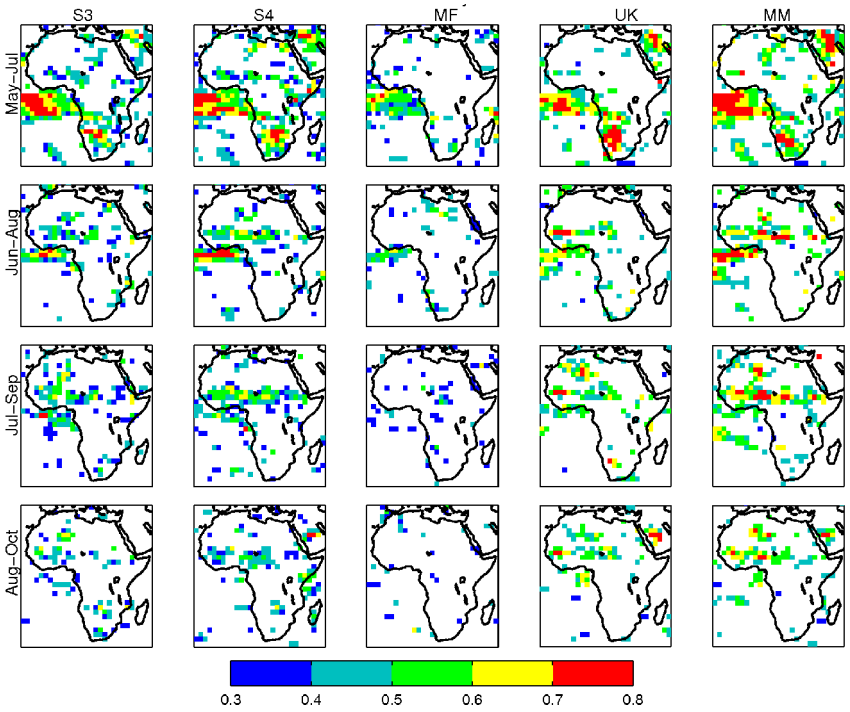

Figure 35. As Figure 9 but for the forecasts starting in May.

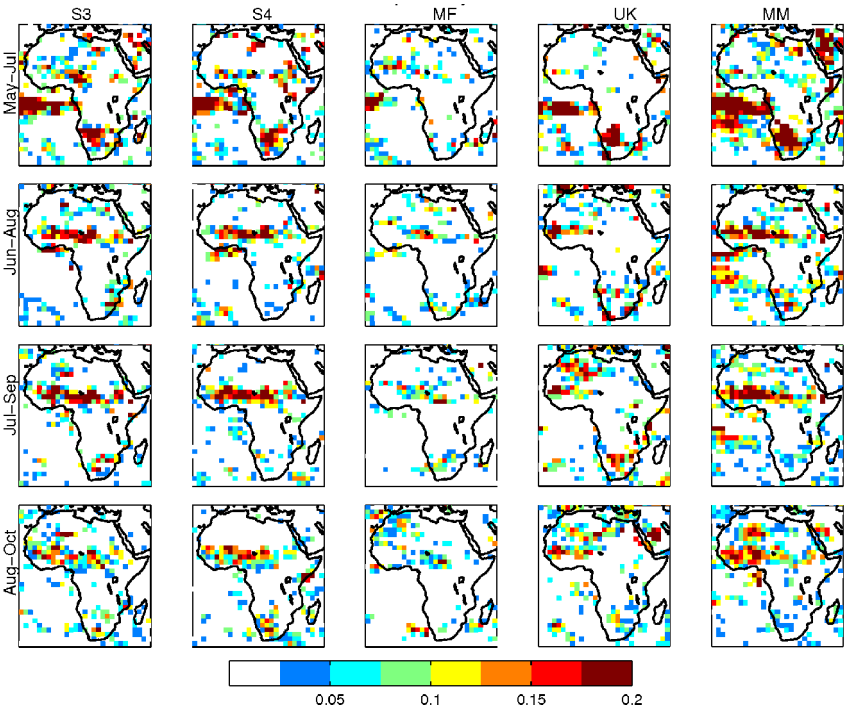

Figure 36. As Figure 10 but for the forecasts starting in May.

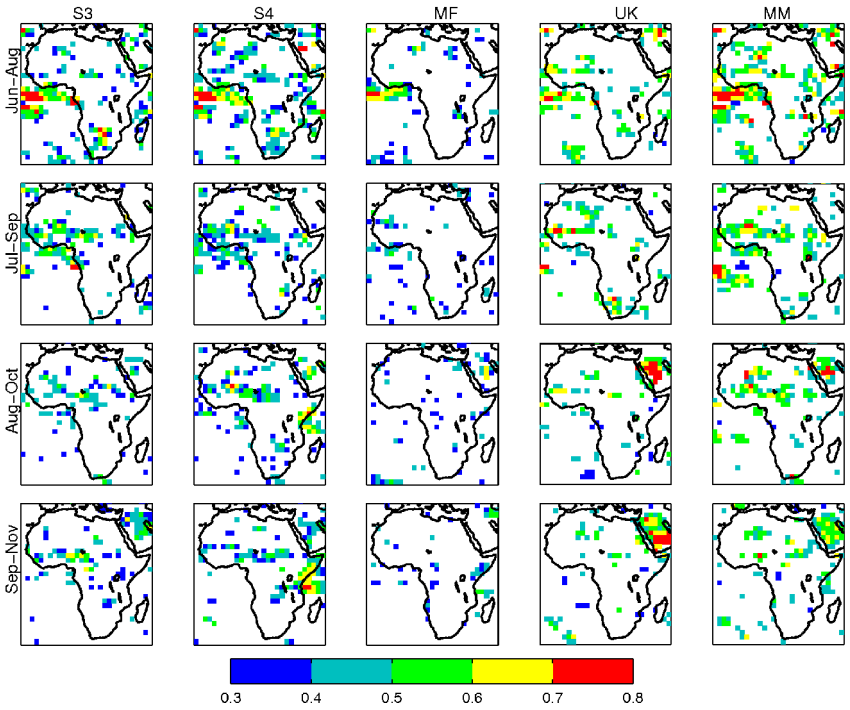

Figure 37. As Figure 9 but for the forecasts starting in June.

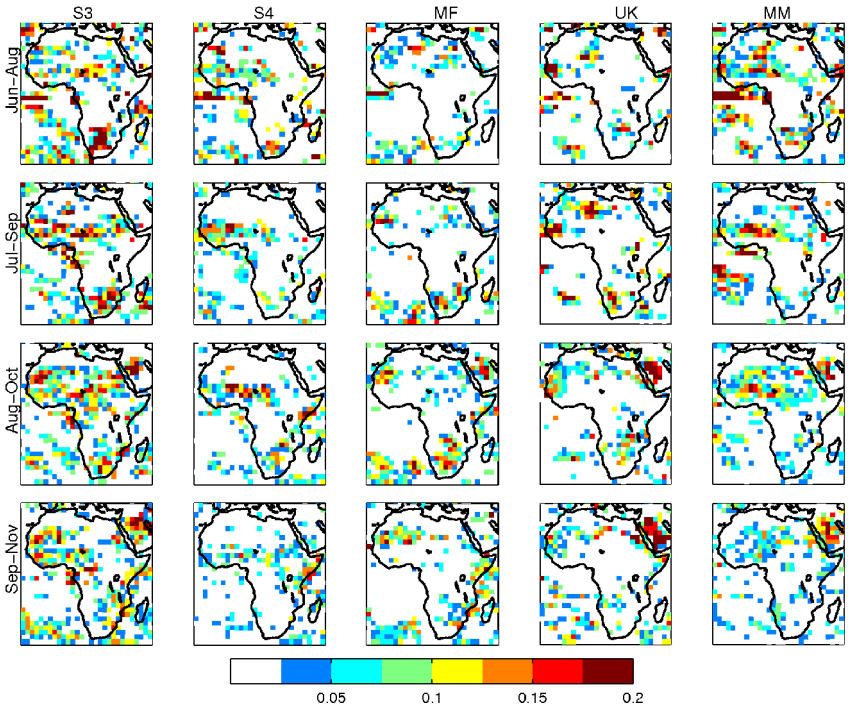

Figure 38. As Figure 10 but for the forecasts starting in June.

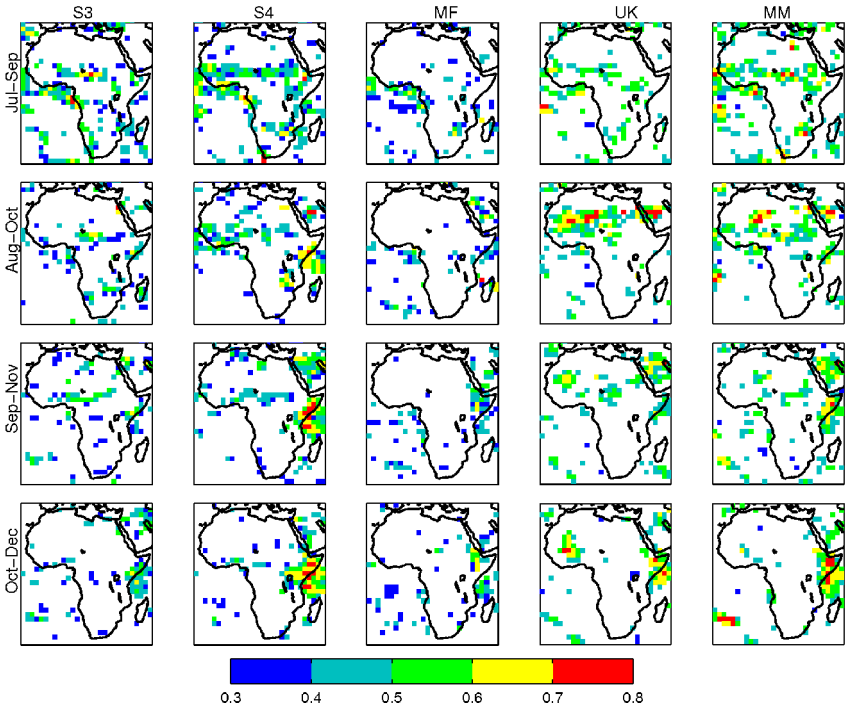

Figure 39. As Figure 9 but for the forecasts starting in July.

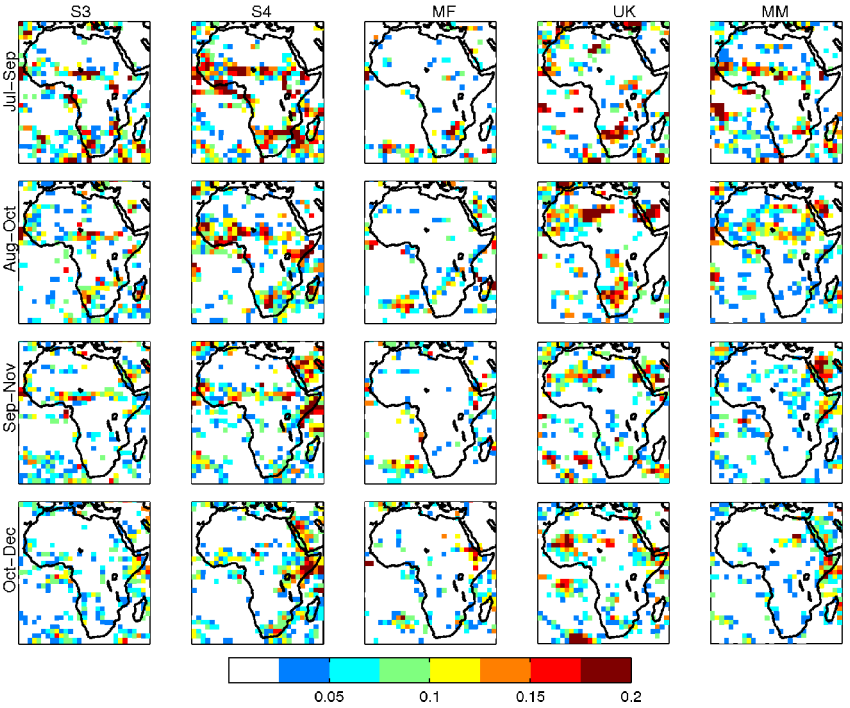

Figure 40. As Figure 10 but for the forecasts starting in July.

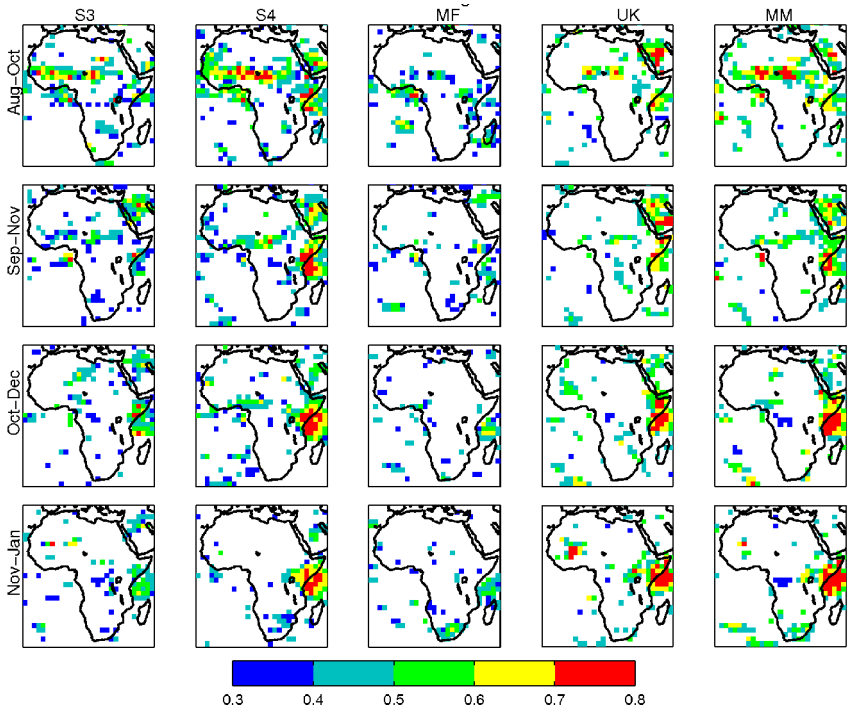

Figure 41. As Figure 9 but for the forecasts starting in August.

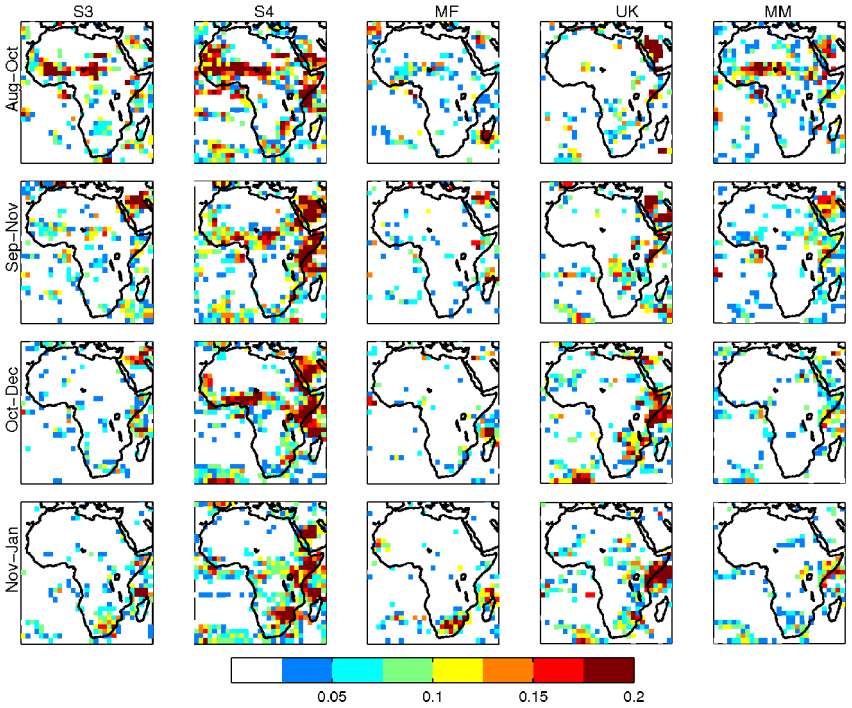

Figure 42. As Figure 10 but for the forecasts starting in August.

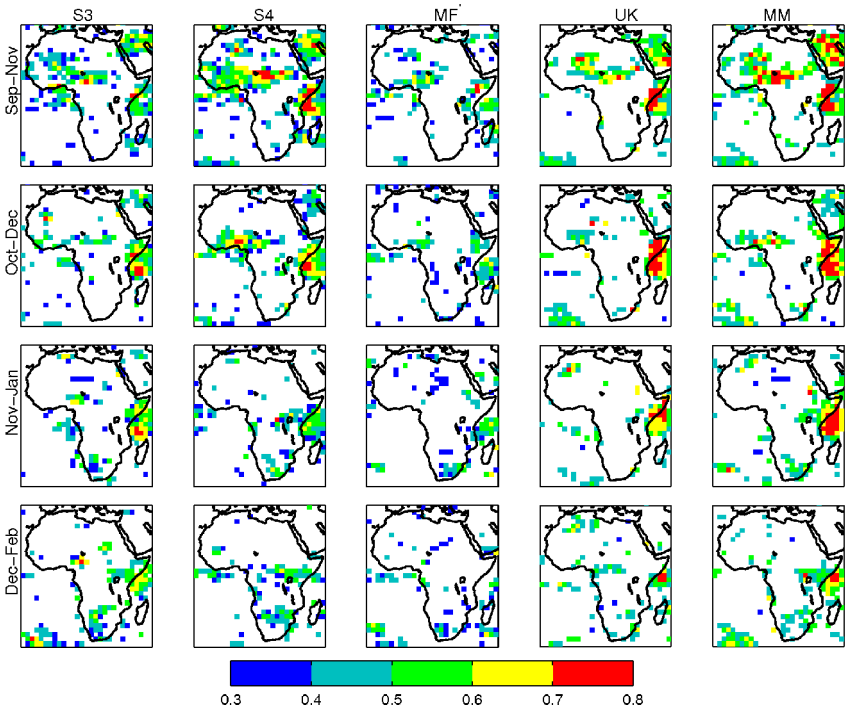

Figure 43. As Figure 9 but for the forecasts starting in September.

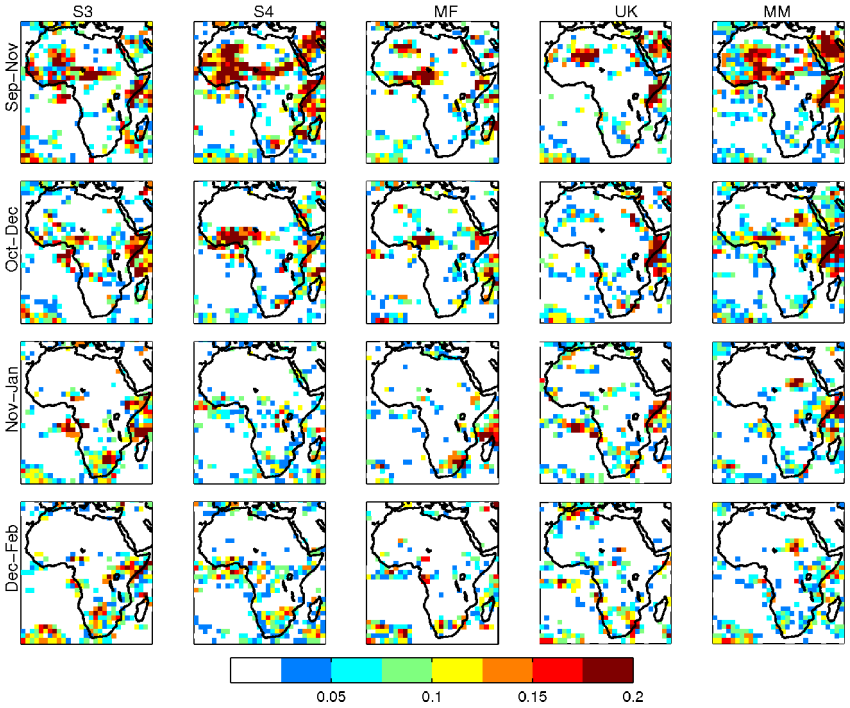

Figure 44. As Figure 10 but for the forecasts starting in September.

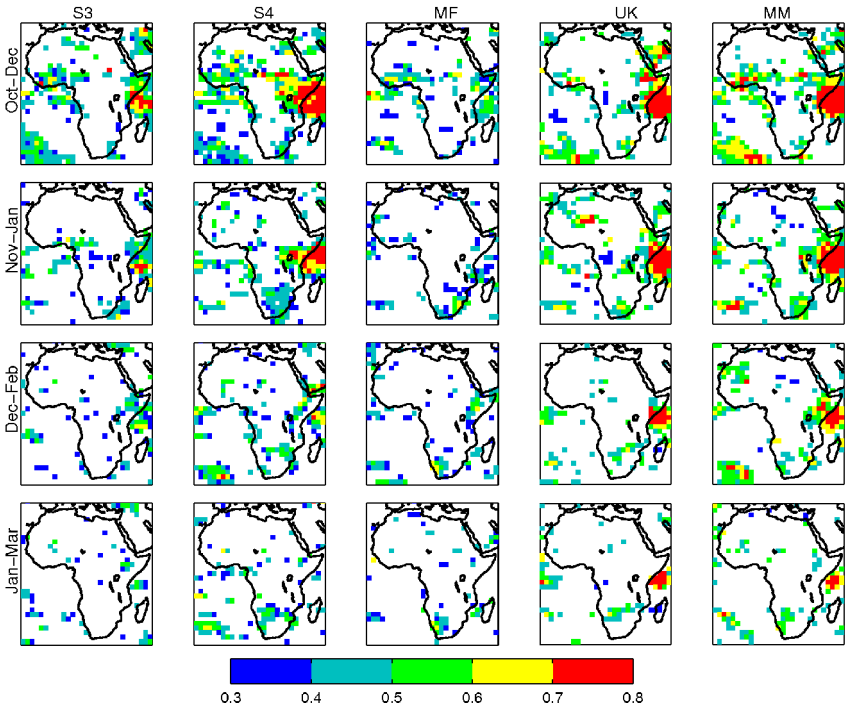

Figure 45. As Figure 9 but for the forecasts starting in October.

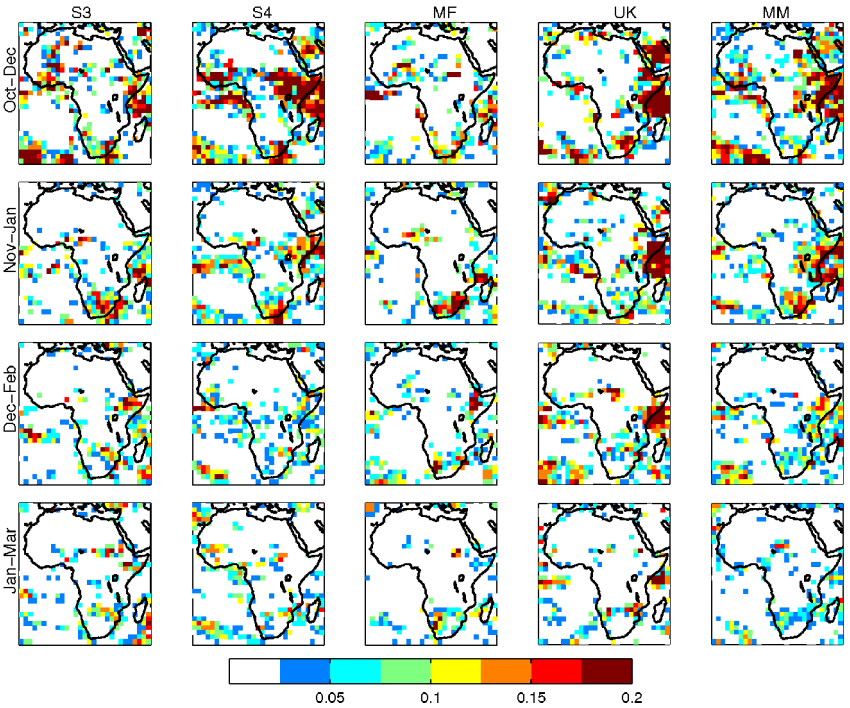

Figure 46. As Figure 10 but for the forecasts starting in October.

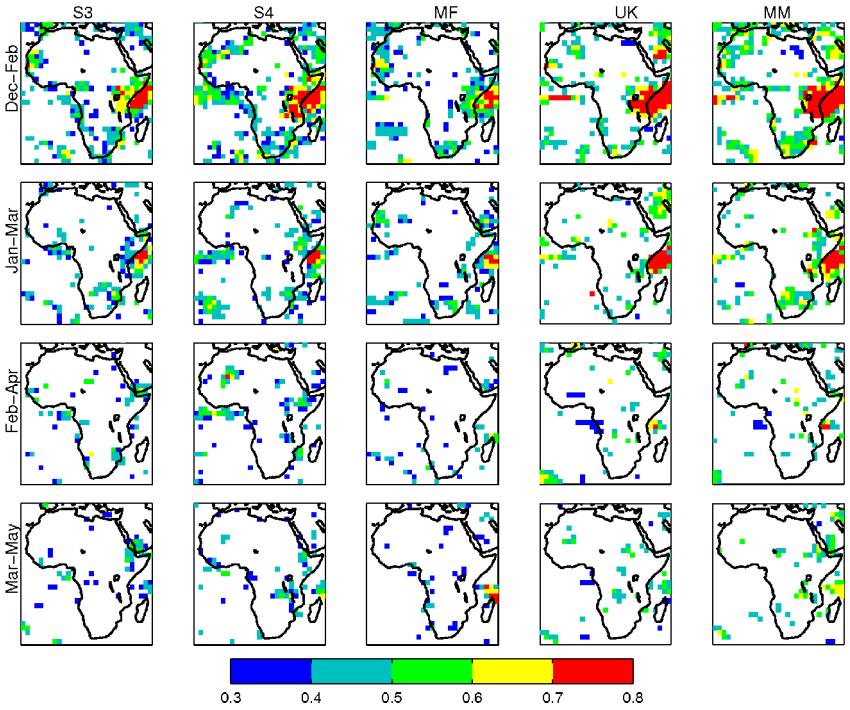

Figure 47. As Figure 9 but for the forecasts starting in December.

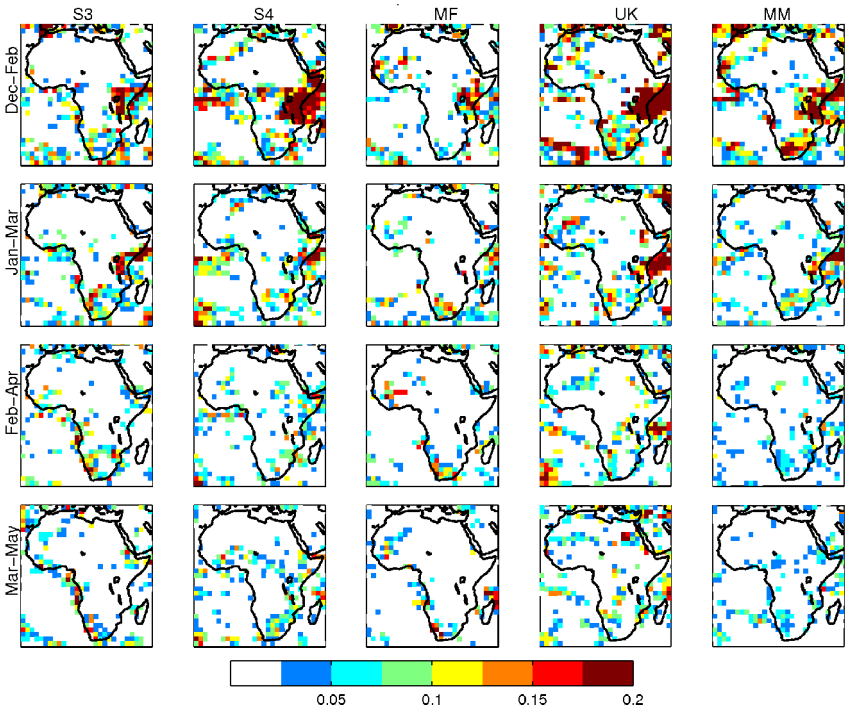

Figure 48. As Figure 10 but for the forecasts starting in December.